

Accepted Manuscript

Anticancer activity of the thiosemicarbazones that are based on di-2-pyridine ketone and quinoline moiety

Anna Mrozek-Wilczkiewicz, Katarzyna Malarz, Marta Rejmund, Jaroslaw Polanski, Robert Musiol



PII: S0223-5234(19)30245-4

DOI: <https://doi.org/10.1016/j.ejmech.2019.03.027>

Reference: EJMECH 11197

To appear in: *European Journal of Medicinal Chemistry*

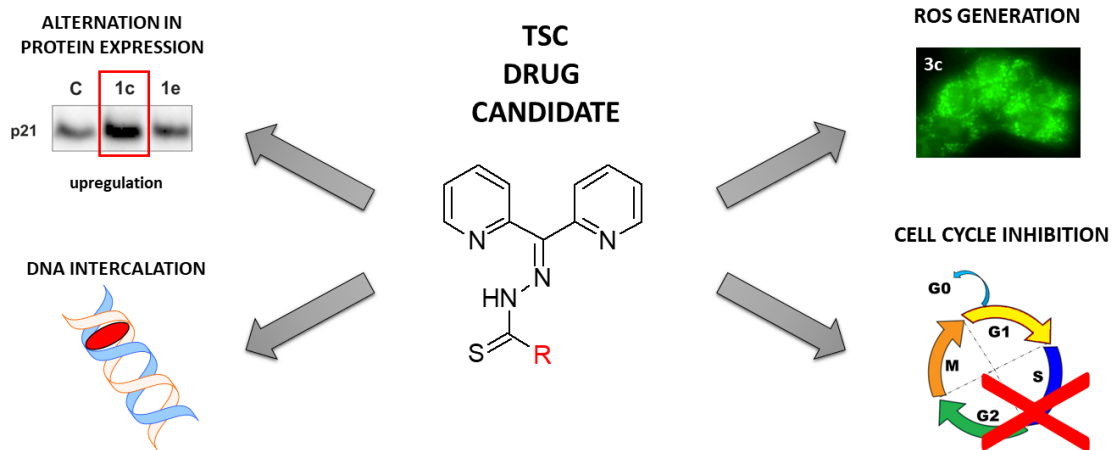
Received Date: 18 December 2018

Revised Date: 7 March 2019

Accepted Date: 11 March 2019

Please cite this article as: A. Mrozek-Wilczkiewicz, K. Malarz, M. Rejmund, J. Polanski, R. Musiol, Anticancer activity of the thiosemicarbazones that are based on di-2-pyridine ketone and quinoline moiety, *European Journal of Medicinal Chemistry* (2019), doi: <https://doi.org/10.1016/j.ejmech.2019.03.027>.

This is a PDF file of an unedited manuscript that has been accepted for publication. As a service to our customers we are providing this early version of the manuscript. The manuscript will undergo copyediting, typesetting, and review of the resulting proof before it is published in its final form. Please note that during the production process errors may be discovered which could affect the content, and all legal disclaimers that apply to the journal pertain.



Anticancer activity of the thiosemicarbazones that are based on di-2-pyridine ketone and quinoline moiety

Anna Mrozek-Wilczkiewicz^{a*}, Katarzyna Malarz^a, Marta Rejmund^b, Jaroslaw Polanski^b and Robert Musiol^b

^aA. Chelkowski Institute of Physics and Silesian Center for Education and Interdisciplinary Research, University of Silesia, Chorzow, Poland

^bInstitute of Chemistry, University of Silesia, Katowice, Poland

*anna.mrozek-wilczkiewicz@us.edu.pl

Keywords: Thiosemicarbazones, anticancer activity, iron chelators, reactive oxygen species, apoptosis, cell cycle inhibition

ABSTRACT

Thiosemicarbazones (TSC) are a subclass of iron-chelating agents that are believed to have an anticancer activity. The high potential for the application of this compound class can be illustrated by a fact that three TSC have entered clinical trials. The ability to chelate metal ions results in several biochemical changes in the cellular metabolism and growth. An important factor that determines the antitumor activity of TSC is a level of iron regulatory proteins and the antioxidant potential that is specific for each type of cancer cell. However, despite the increasing interest in TSC, their mechanism of anticancer activity is still unclear. For a more effective and rational design, it is crucial to determine and describe the abovementioned issues. In this report, we describe a series of new TSC that are designed on the four main structural scaffolds. The anticancer activity of these compounds was evaluated against a panel of cancer cell lines including colon and breast cancers and gliomas. Special attention was paid to the metal-dependent proteins. The impact of the tested TSC on the cell cycle and redox homeostasis was also determined. These results confirm a p53-independent mechanism of apoptosis.

1. Introduction

Thiosemicarbazone derivatives (TSC) are commonly known for their wide biological activity, which includes their anticancer, antimicrobial and antiviral properties [1]. Interest in this family of compounds has increased significantly over the years from the very first report in 1950 to the thousands of papers that were published in 2017. Currently, the anticancer activity of TSC is being most extensively investigated and several drug candidates are entering the clinical phase [2]–[4] (NCT02688101, NCT00004213, NCT02433626). A leading TSC compound, Triapine (**3-AP**), was carefully investigated in clinical phase I and II trials. The research indicated that this TSC alone or in a combination with gemcitabine, cisplatin or radiation effectively inhibits the growth of different types of tumors (NSC #663249, IND # 68338). Surprisingly, despite such dynamic progress and the many papers that describe the molecular mechanism of the action of this family of compounds, there are still many gaps in the complete understanding of their high anticancer activity.

The inhibition of cancer cell proliferation that is caused by TSC is connected with several factors such as the deactivation of the ribonucleotide reductase (RR) enzyme [5], cell cycle inhibition [6], reactive oxygen species (ROS) generation [7], the chelation of important metal ions [8] and its influence on the proteins that are crucial in life and death processes of cells [9], [10]. The issue is complex enough to explain consistent mechanism of action or even general remarks on target specificity. On the other hand, individual features of the cancer types may change the cellular reaction to TSC and the outcome of therapy. Other less frequently addressed features that affect the landscape of TSC activity are their own structural features. This is more evident in a wide group of iron chelators in which the nature of the complexes determines the susceptibility to the Fenton reaction and thus the generation of ROS. Thiosemicarbazones produce ROS by switching between the different oxidation states of the metal ions in the redox reaction. For example, iron ions exist in the form Fe^{2+} and Fe^{3+} and these forms participate in the redox reaction. The binding of the metal ion by a ligand (TSC), that does not saturate its coordination sites may allow or even facilitate the redox cycle. This ability could be changed by the donor atoms that form a coordination bond with the metal [11]. This is also why fully coordinating chelators such as DFO do not generate ROS [12], [13]. Lovejoy et al. conducted an experiment with the preincubation of cells with a strong chelator that binds the metal ions in a cell. After the incubation with the active TSC, there was no cytotoxic effect, which means that metal chelation is essential for the activity of TSC [14].

With the expansion of the TSC class, it has become clear that this group is heterogeneous enough to reveal some distinct variability in the mechanism of action. Prime

examples are **3-AP** and **Dp44mT** whose different mechanisms were published [15]. The debate is still ongoing as a topoisomerase inhibitory activity was suggested for **Dp44mT** [6], which was previously verified [16]. As we have actively worked in this scientific field for some time, we found it quite confusing and worth putting more effort into clarifying this situation. Therefore, in the present work, we selected seventeen newly synthesized TSC (**Fig. 1**) from four of the most frequently described groups and evaluated their activity profile. Compounds (**1a-e**), which have a dipyridyl moiety, are among the most active TSC [17], [18]. A second important group are Triapine and its analogs, which are built on one pyridine ring (**2a-c**) [2], [8]. Quinoline (**3a-h**) and quinazoline (**3i, 3j**) derivatives have been developed on the basis of their multicenter chelating ability and have also provided several active agents [19]–[22].

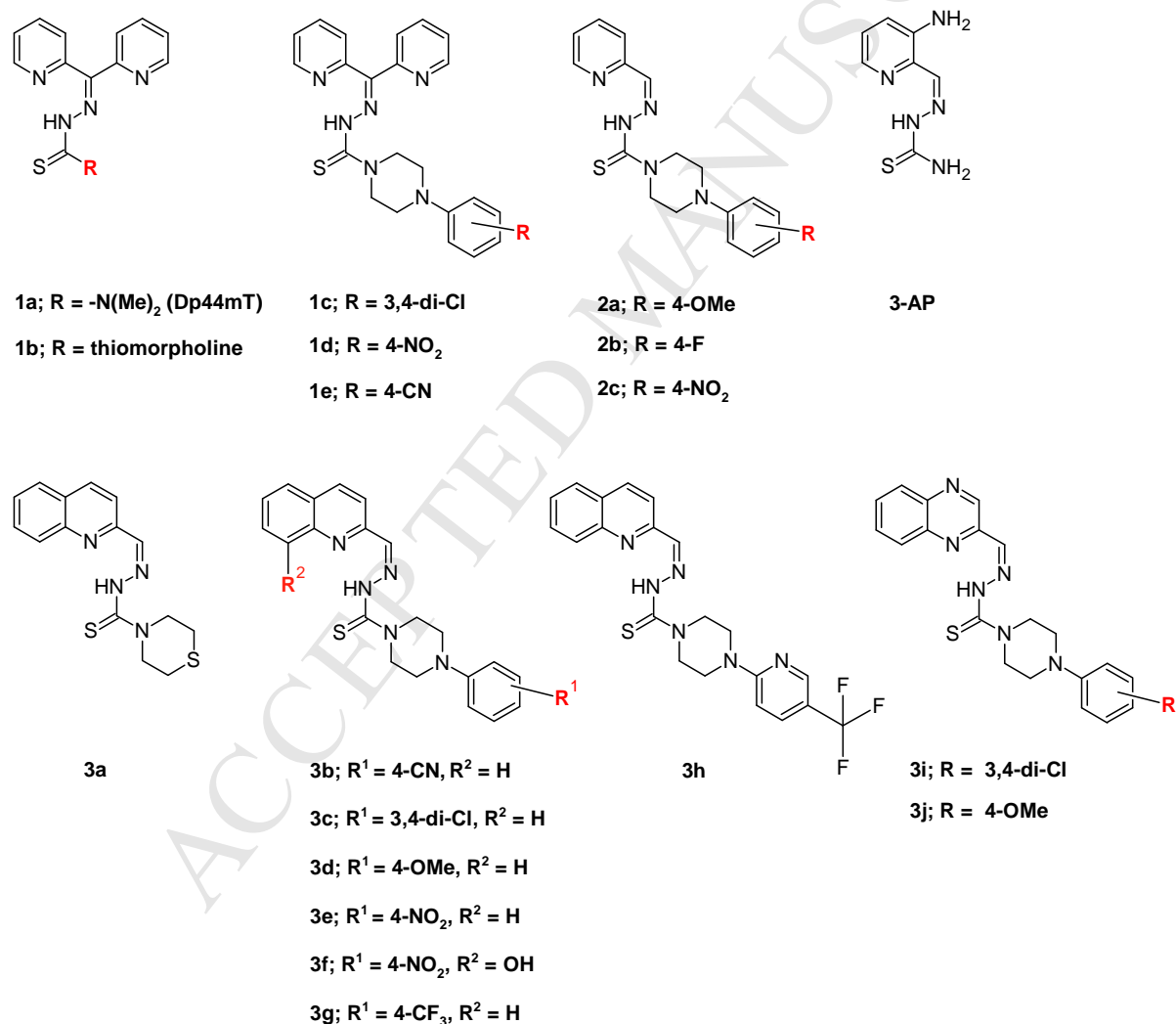


Figure 1: Structures of the studied compounds.

2. Results and discussion

2.1. Chemistry

The synthesis of the TSC was carried out according to known procedures. Compounds **1a-e**, which were built on a dipyridyl moiety, were obtained from ketone and appropriate amines as was described earlier [20]. The pyridine thiosemicarbazones **2a-c** were synthesized from pyridine thiosemicarbazide as reported earlier [8]. The quinoline and quinoxaline aldehydes were used to form the corresponding derivatives **3a-j**.

2.2. Cytotoxicity studies

Iron chelators have gained strong interest for their high level of activity and multitarget mechanisms of action. After an initial success, **3-AP** appeared to cause side effects such as methemoglobinemia. The next generation of TSC that are di-substituted at a terminal amine group (N4) were extensively investigated by the Richardson's group [23]–[25]. Among them, the derivatives of di-2-pyridylketone were the most active with **Dp44mT** and an analog with a cyclohexyl substituent in the amine group (**DpC**) as prime examples [26]. A series of derivatives with alkyl and an aryl substituents in the amine group were investigated for **DpT** (di-2-pyridine) and **BpT** (2-benzoylopyridine) thiosemicarbazones [17], [27]. Interestingly, although an alkyl substitution is beneficial for the activity, their increasing lipophilicity has a rather detrimental effect [10]. Consequently, larger, but still reasonably lipophilic morpholine and phenylpiperidine (as in COTI-2) substituents, may result in active compounds [20], [28], [29].

Our current report combines several structural groups of the TSC family that confirm this trend. In general, all of the compounds were active against all of the cancer cell lines. Moreover, their activity was at least two orders of magnitude higher than Triapine. For the characterization of the antiproliferative activity of all of the newly synthesized derivatives, **1a-e**, **2a-c**, and **3a-j**, we selected six cell lines that represent different human tumors and one normal fibroblast line. We focused on colon (HCT 116; p53^{+/+} and p53^{-/-}) and breast cancers (MCF-7), which are some of the most common type of tumors. Additionally, we also selected gliomas (U-251, Hs 683), which are particularly dangerous due to their aggressiveness and the fact that they are difficult to treat. To determine the selectivity index, we selected normal human dermal fibroblasts (NHDF). In our research, we explored the effect of the p53 tumor suppressor protein on inhibiting cell growth. It is commonly known that more than 50% of cancers have a mutation in the *TP53* gene. P53 is a cell-protecting protein that plays the role of a genome guard. Cancers that have a mutation in this protein are more aggressive and are prone to drug resistance. The prognosis for these tumors is also poor [30]. In our experiments,

we selected two cell lines that had alterations in *TP53* gene. Namely, a colon carcinoma with a double-deletion HCT 116 – p53^{-/-}, which loss of the p53 function as well as a glioblastoma U251, which expressed a point missense mutation that changed arginine to histidine at codon 273. The latter mutation has been revealed to be potentially more oncogenic for targeting the protein to the nucleus [31]. As is presented in **Table 1**, all of the compounds that were synthesized showed good activity against all cancer cell lines, which was higher than **3-AP**. The IC₅₀ values varied from 0.01 μM (compound **2c** on HCT 116 p53^{-/-}) to values that can be considered to be inactive (>25 μM). For better clarity, we used a color code map to distinguish between the highly active (IC₅₀ <1 μM, marked as red), active (IC₅₀ 1-6.25 μM, marked as yellow) and inactive (IC₅₀ >6.25 μM marked as grey) compounds. Their activity against fibroblasts was used to determine the selectivity indexes (SI) of each cell line. These data are presented in **Table S1** in the **Supporting Information**.

IC₅₀ < 1 μM
 IC₅₀ 1 - 6.25 μM
 IC₅₀ > 6.25 μM

Table 1: Antiproliferative activity of the studied compounds.

Comp.	Activity - IC ₅₀ [μM]					
	HCT 116 p53 ^{+/+}	HCT 116 p53 ^{-/-}	MCF-7	U-251	Hs 683	NHDF
3-AP	1.12 ± 0.28	1.34 ± 0.34	2.33 ± 0.43	1.48 ± 0.56	1.76 ± 0.29	>25
1a (Dp44mT)	0.00123± 0.00018 1.23·10 ⁻³ ± 0.18·10 ⁻³	0.00110± 0.00006 1.10·10 ⁻³ ± 0.06·10 ⁻³	0.00114± 0.00040 1.14·10 ⁻³ ± 0.40·10 ⁻³	0.00114± 0.00006 1.14·10 ⁻³ ± 0.06·10 ⁻³	0.00396± 0.00070 3.96·10 ⁻³ ± 0.70·10 ⁻³	18.88 ± 1.59
1b	0.84 ± 0.19	0.18 ± 0.02	0.19 ± 0.04	0.20 ± 0.02	0.45 ± 0.19	10.30 ± 1.07
1c	0.31 ± 0.06	0.015 ± 0.004	0.07 ± 0.02	0.15 ± 0.04	0.17 ± 0.03	12.87± 0.99
1d	3.20 ± 1.32	0.14 ± 0.02	0.16 ± 0.05	0.19 ± 0.04	0.56 ± 0.28	>25
1e	0.23 ± 0.15	0.019 ± 0.003	0.034 ± 0.008	0.28 ± 0.09	0.48 ± 0.19	12.32 ± 0.37
2a	5.13 ± 1.24	0.23 ± 0.08	0.54 ± 0.10	0.19 ± 0.05	6.95 ± 3.65	>25
2b	0.17 ± 0.05	0.014 ±	0.015 ±	0.021 ±	0.51 ± 0.29	>25

		0.004	0.006	0.006		
2c	0.30 ± 0.07	0.010 ± 0.003	0.021 ± 0.006	0.036 ± 0.007	4.68 ± 2.86	13.28 ± 0.56
3a	18.31 ± 0.92	5.85 ± 0.45	-	-	-	13.06 ± 1.9
3b	0.56 ± 0.14	0.43 ± 0.03	0.23 ± 0.11	0.18 ± 0.06	6.33 ± 1.61	>25
3c	0.16 ± 0.05	0.15 ± 0.06	0.09 ± 0.01	0.47 ± 0.05	8.52 ± 2.14	14.74 ± 0.79
3d	1.10 ± 0.33	0.065 ± 0.004	0.03 ± 0.01	0.05 ± 0.01	0.28 ± 0.09	0.28 ± 0.05
3e	5.10 ± 1.79	0.22 ± 0.02	0.31 ± 0.09	5.54 ± 1.49	14.81 ± 0.72	3.22 ± 0.77
3f	11.69 ± 1.77	8.42 ± 1.33	-	-	-	>25
3g	0.14 ± 0.01	0.07 ± 0.02	0.07 ± 0.02	0.17 ± 0.02	0.22 ± 0.06	12.09 ± 0.61
3h	0.18 ± 0.04	0.14 ± 0.05	0.07 ± 0.02	0.13 ± 0.04	0.27 ± 0.06	16.66 ± 5.57
3i	1.06 ± 0.14	0.29 ± 0.08	0.50 ± 0.14	1.19 ± 0.32	3.62 ± 1.16	21.34 ± 1.34
3j	5.47 ± 1.19	6.27 ± 1.95	-	-	-	>25

The greatest activity among the newly synthesized compound was shown by pyridine derivative **2c** (IC_{50} on HCT 116 p53^{-/-} equals 0.010 μ M). The activity dramatically decreased (30 times) for the wild-type HCT 116. Compound **2c** primarily inhibited the proliferation of the MCF-7 (IC_{50} = 0.021 μ M), and U-251 (IC_{50} = 0.036 μ M) cells while the Hs 683 cells were rather resistant (IC_{50} = 4.68 μ M). This trend (p53 influence) was observed for all of the investigated derivatives except **3b**, **3c** and **3h**, which had little or no difference in IC_{50} against both colon carcinoma lines. This observation is particularly important because to date almost no similar findings have been reported for TSC. To the best of our knowledge, TSC iron chelators have not been distinguished between the wild-type and p53 null cell lines [8], [20], [22], [32]. Only a few, sporadic quinoline-based compounds that exhibit a preference to HCT 116 p53^{-/-} have been published to date [21]. What is even more interesting is that most of the compounds presented in **Table 1** are also highly active against U251. Only **1c**, **3g** and **3h** have no preference for the brain tumor cell lines. Thus, this is the first evidence that a change in the *TP53* gene in cancer cells may result in an increasing susceptibility to chemotherapy with some TSC. The next most active compound was **2b**, which also had the greatest effect on HCT 116 p53^{-/-} (IC_{50} = 0.014 μ M). In this case, along with a prior observation, we observed a decrease in the activity (12 times) in response to the incubation with HCT 116 p53^{+/+} as well.

For this compound, we also observed a considerable inhibition of the proliferation of the MCF-7 ($IC_{50} = 0.015 \mu\text{M}$) and U-251 ($IC_{50} = 0.021 \mu\text{M}$) cells and a moderate effect on the Hs 683 cells ($IC_{50} = 0.51 \mu\text{M}$). Compound **1c** had a very similar pattern of the inhibition of the proliferation of selected cell lines and, additionally, this compound was the best inhibitor of the Hs 683 cells ($IC_{50} = 0.17 \mu\text{M}$). In the light of that observation it is quite interesting that gliomas are one of the most treatment-resistant tumors.

Crystal structures show that a metal atom is complexed through three atoms of a ligand – N (from the pyridine ring) and N and S (from the thiosemicarbazone group) [33]. The nitrogen from the terminal amine group does not participate in chelating, but it still has an impact on the cytotoxic activity. Double-alkylation as in **Dp44mT**, **DpC** and other highly active TSC increases the basicity of the N4 atom or the relative lipophilicity of a molecule [10], [34]. Stacy et al. reported that **Dp44mT**, but not **3-AP**, penetrates the lysosomes and forms complexes that have a high redox potential with Fe or Cu [35]. Further permeabilization through the lysosome membrane leads to an initiation of the autophagic pathway [36], [37]. Moreover, the importance of an electron-withdrawing group at the imine carbon of the thiosemicarbazone moiety (as in a **DpT** series) has also been indicated. This has an influence to lipophilicity, which in addition to its basic character is crucial to being sequestered by lysosomes [35].

Conversely, in a recent report of Hager and coworkers, a Triapine derivative (Me_2NNMe_2) that was obtained *via* the double methylation of both amine groups appeared to be active at nanomolar concentrations [38]. However, the mechanism of action that was revealed consists of the inhibition of the protein disulphide-isomerase (PDI). Importantly, this mechanism has been confirmed by *in vitro* assays, which showed that the Cu-complex of Me_2NNMe_2 , but not Triapine, effectively inhibits the PDI enzyme. This may suggest that the dimethylamine group is crucial for the ligand-protein interaction at least for some TSC.

In our series **1** compounds, we observed that the activity can be reversely correlated with the electron-withdrawing effect of the substituent in the phenylpiperazine moiety. The derivative **1d** with the strongest electron-accepting para-nitro group was the least active compound in this group. Compound **1b**, which is the closest derivative of our reference **Dp44mT** (**1a**), deserves more attention as well. The substitution with a morpholine ring caused a significant decrease in the activity of **1b** against all of the cancer cell lines that were tested. As was presented by Serda et al. the morpholine and piperazine derivatives of **Dp44mT** can be active (IC_{50} is ten times lower) against both HCT 116 cell lines [20]. In the current study, thiomorpholine compound **1b** was significantly less active than **Dp44mT**

against HCT 116 cell lines (700 and 180 times respectively). The detrimental effect of heterocyclic sulphur was also visible in the quinoline-based compound **3a**, which was completely inactive in this series.

A comparison of the activity of series **1** and **2** led to the conclusion that similar structural effects promote the cytotoxic activity in both series. The electron-withdrawing substituents in the phenyl ring are crucial for the activity (compare the methoxy- **2a** and nitro- **2c**). However, the pyridine derivatives were generally slightly more active (**1d** vs. **2c**).

In series **3**, which was based on the quinoline moiety, we observed the greatest diversity in biological activity. The thiomorpholine derivative **3a**, which opens this family and compound **3f** are the least active in this series. In turn, the conversion of the thiomorpholine ring into a phenylpiperazine tail significantly improved its activity. Derivative **3d** was the fifth most active compound among the 18 investigated TSC. IC_{50} fluctuated in the range of 0.031-0.065 μ M for MCF-7, U-251 and HCT 116 p53^{-/-}, respectively. The effect of the p53 protein on the response to treatment was the most noticeable for **3d**. This compound was 35 times more active on the HCT 116 that had a deletion of the *TP53* gene than on the wild type that had an active p53 protein (IC_{50} = 0.065 vs. 1.10 μ M). Similarly, it also had a high level of activity against the second p53-mutant U251 cell line. The substitution of the OMe group on 4-CN, 3,4-di-Cl or 4-CF₃ caused a loss of selectivity (**3d** vs. **3b**, **3c**, **3g**, and **3h**). Among the series **3** compounds, **3f** and **3j** (together with **3a**) were the least active. This may indicate that the OH group might be a steric hindrance for metal binding (**3e** vs. **3f**). Moreover, the addition of the N atom in the quinoline ring had a negative effect on its activity (**3c** vs. **3i**, **3d** vs. **3j**). This observation confirms the effect of the electron-accepting effect of the substituents in the phenylpiperazine fragment that was observed for mono- and dipyrindine TSC. Compounds **3g** and **3h**, which had an electron-withdrawing group CF₃, had a high level of activity. On the other hand, the non-selective **3d** that had an electron-donating methoxy group was also active (but not against HCT 116 p53^{+/+}). The lower level of activity of the nitro or cyano derivatives might be explained on the basis of their lower lipophilicity compared to the trifluoromethyl or dichloro derivatives.

The selectivity indexes for all of the selected cell lines are presented in **Table S1** (Supporting Information). Despite their high level of anticancer activity, the calculated SI were high, which makes the investigated TSC promising candidates for further research.

2.3. Cell cycle assay

The interesting antiproliferative profiles prompted us to explore the mechanism of action in more detail. The cytotoxicity results, which were discussed earlier, suggest a p53-independent mechanism of action. To evaluate this hypothesis, we decided to perform a more in-depth investigation of three cell lines; HCT 116 p53^{+/+}, MCF-7 and U-251. The most active compounds in those cells were selected. In the first step, we measured the effect of the tested compounds on the cell cycle. The results of these experiments are presented in **Fig. 2**, and **Fig. S1, S2**. In all of the cases, we detected the effect of the tested compounds on the cell cycle phase, which was most pronounced in the HCT 116 cells (**Fig. 2**). The population of cells decreased (compared to the control) in the G0/G1 phase after treatment with all of the tested compounds. The decrease reached more or less 10-20%. The reverse occurred in the case of the S phase where we observed an increase in the cell population from 17 to 23% (**2c**). For the G2/M phase, we detected a similar situation – the highest growth rate was 10% for **3h**, while this was in the range 2-10% for the rest. These observations suggest that investigated compounds inhibit the cell cycle in the S or G2/M phases.

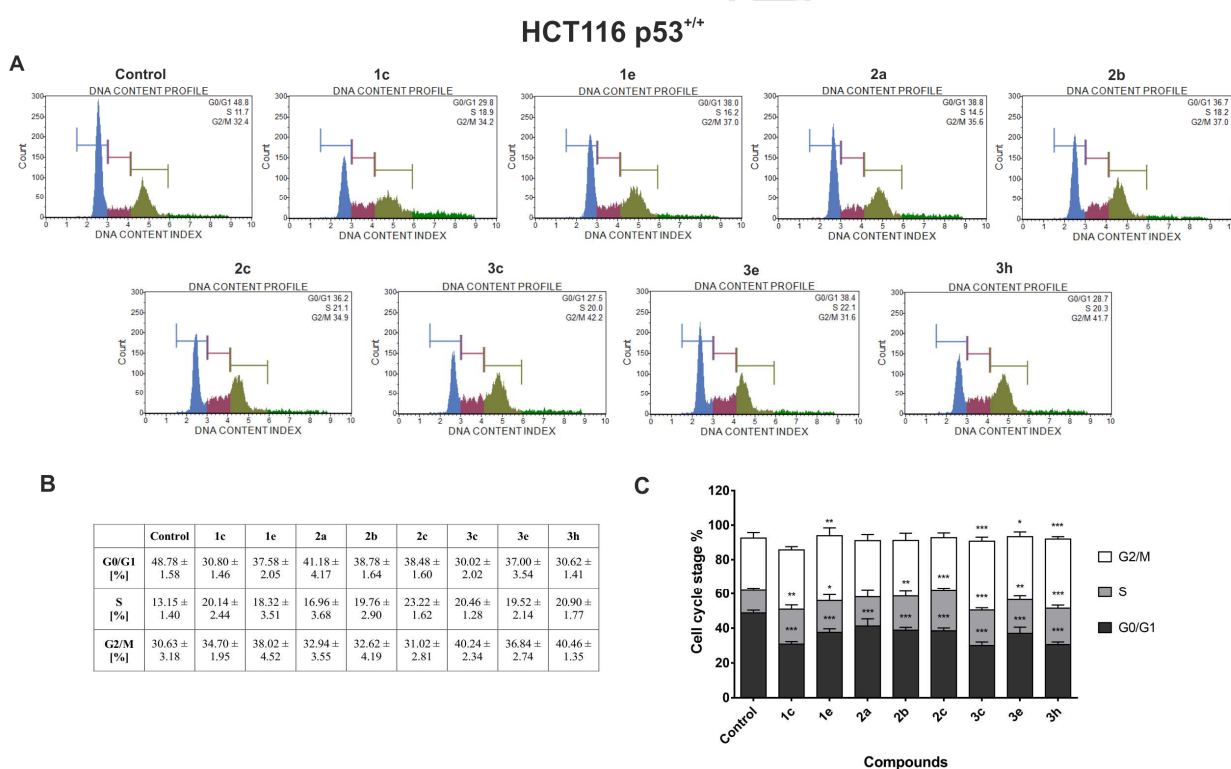


Figure 2: Effect of the tested TSC (0.5 μ M) on regulating the cell cycle in HCT 116 cells. The histograms show the distribution of the cells in the G0/G1, S and G2/M phases of the cell cycle for one of the experiments (**A**). The table shows the mean \pm SD percentage of the cells in the G0/G1, S and G2/M phases of the cell cycle from three independent experiments (**B**).

The data were analyzed using one-way ANOVA with a Bonferroni's post-hoc test: * $p < 0.05$, ** $p < 0.01$, *** $p < 0.001$ compared to the control (C).

In the case of the next analyzed cell lines – MCF-7 and U-251, we observed a similar but less visible trend (**Fig. S1, S2**). A decrease in the cell population in G0/G1 phase and an increase in the S and G2/M phases suggest that all of the tested compounds inhibit proliferation in the S and G2/M phases.

2.4. Annexin V binding assay

The next step was to evaluate the type of cell death. We performed the assay based on measurements of the apoptotic cells by counting the fluorescence of FITC conjugated to Annexin V. Only cells that had a disintegrated cell membrane emitted the green signal. For this experiment, we selected the same three cell lines as were discussed above – HCT 116, MCF-7 and U-251 (**Fig. 3, and S3, S4**). In general, we observed the strongest effect for the **3h** derivative (76.18% of the apoptotic cells for MCF-7, **Fig. S3B, C** and 64.81% for HCT 116, **Fig. 3B, C**). In the HCT 116 cells, a large number of apoptotic cells were observed for all of the derivatives (60.32-39.39%) and a moderate number for the rest (**2a** and **3e**). These results correlate well with the IC_{50} values for these compounds. In MCF-7, we also detected a strong apoptotic effect (57.60-22.30%) for all of the compounds except **3e**. For U-251, the population of apoptotic cells was smaller and ranged from 30.34 to 13.33%. The smallest population was observed for **2a** and **3e** (**Fig. S4**).

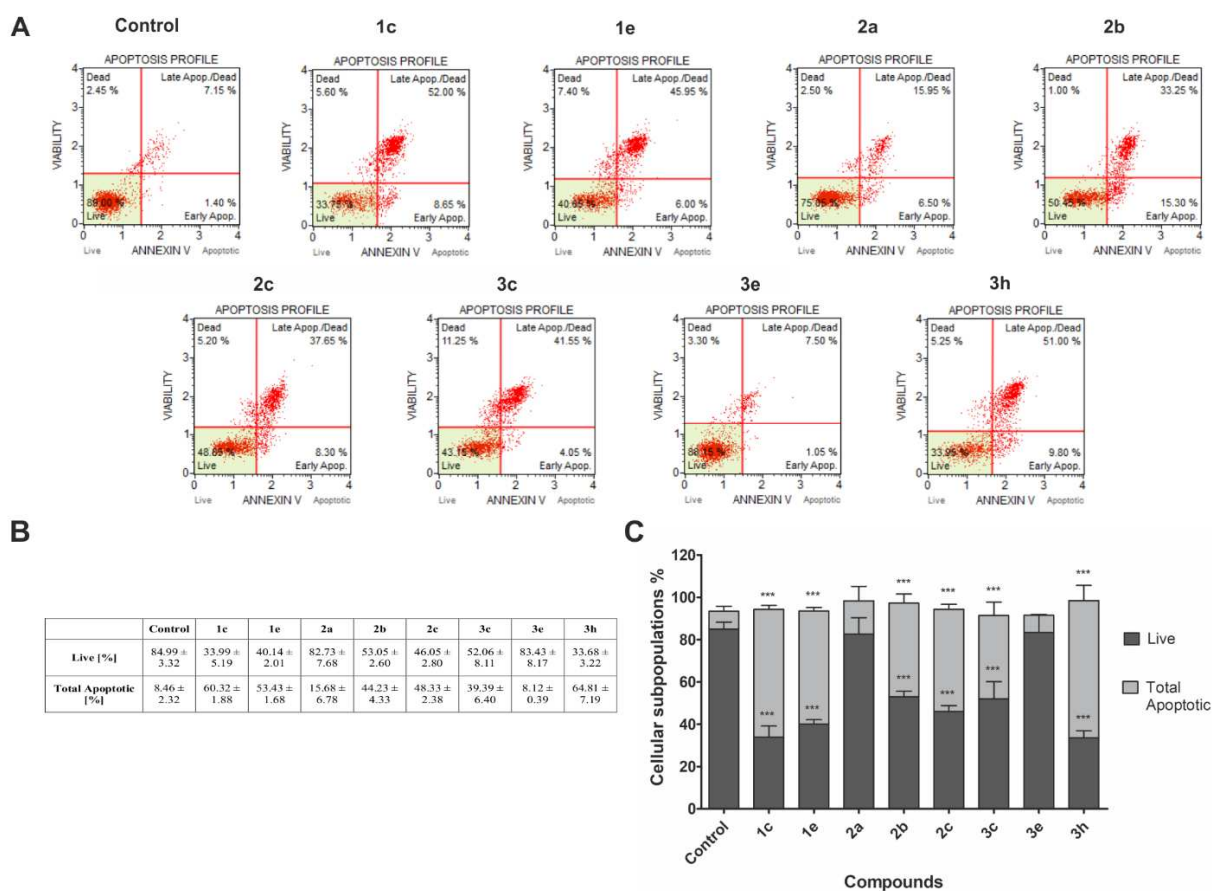
HCT116 p53^{+/+}

Figure 3: Evaluation of the induction of apoptosis in the HCT 116 cells after a 48-h treatment with TSC (0.5 μ M). The histograms show the percentage of early and late apoptosis for one of the experiments (A). The table shows the mean \pm SD percentage of the live, early and late apoptotic cells from three independent experiments (B). The data were analyzed using one-way ANOVA with a Bonferroni's post-hoc test: * $p < 0.05$, ** $p < 0.01$, *** $p < 0.001$ compared to the control (C).

2.5. Immunoblotting

As was mentioned above, all of the compounds had a greater biological activity on the cells that have a mutation or deletion of the *TP53* gene. To further evaluate the hypothesis of a p53-independent mechanism of apoptosis, we measured the expression of the proteins that are crucial in the proliferation and activation of cell death. The levels of p53, p21, cytochrome c, cdc2, cyclin D1 and PARP were identified using a Western blot assay on HCT 116 p53^{+/+} and MCF-7. The results are shown in **Figures 4** and **5**.

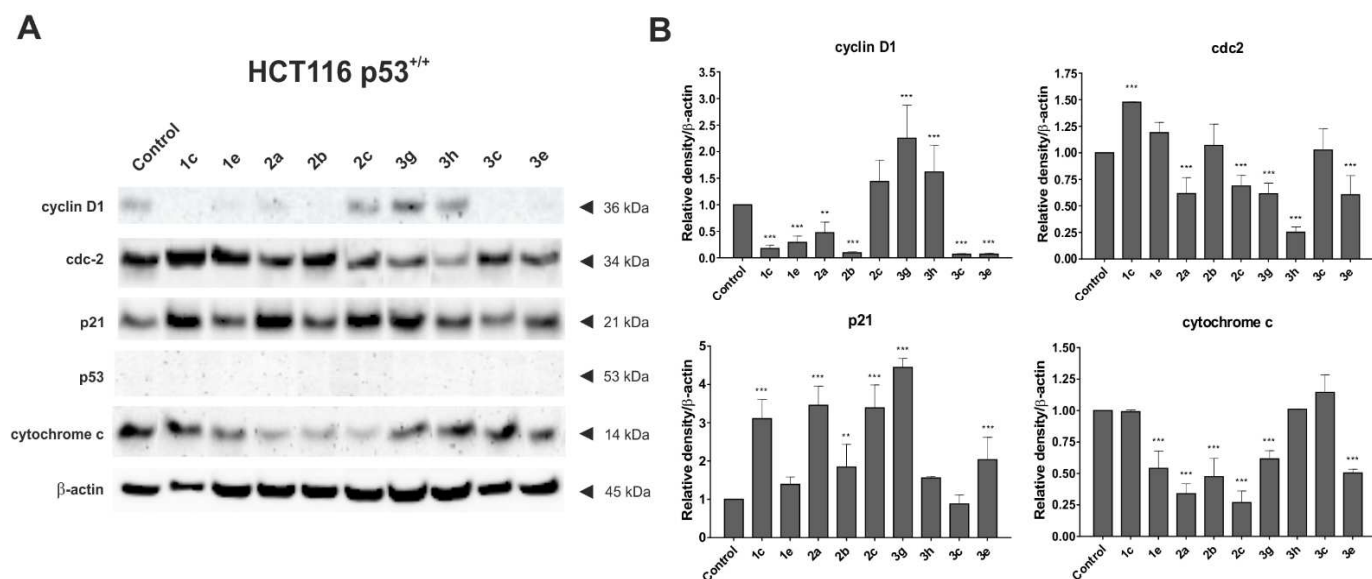


Figure 4: Effect of the tested TSC (concentration $4 \times IC_{50}$) on the expression of the cell cycle and apoptosis proteins in the HCT 116 cells (**A**). The densitometric analyses of cyclin D1, cdc2, p21, p53 and cytochrome c were normalized to β -actin. The results are the mean \pm SD of five independent experiments. Statistical differences were analyzed using one-way ANOVA with a Bonferroni's post-hoc test: * $p < 0.05$, ** $p < 0.01$, *** $p < 0.001$ compared to the control group (**B**).

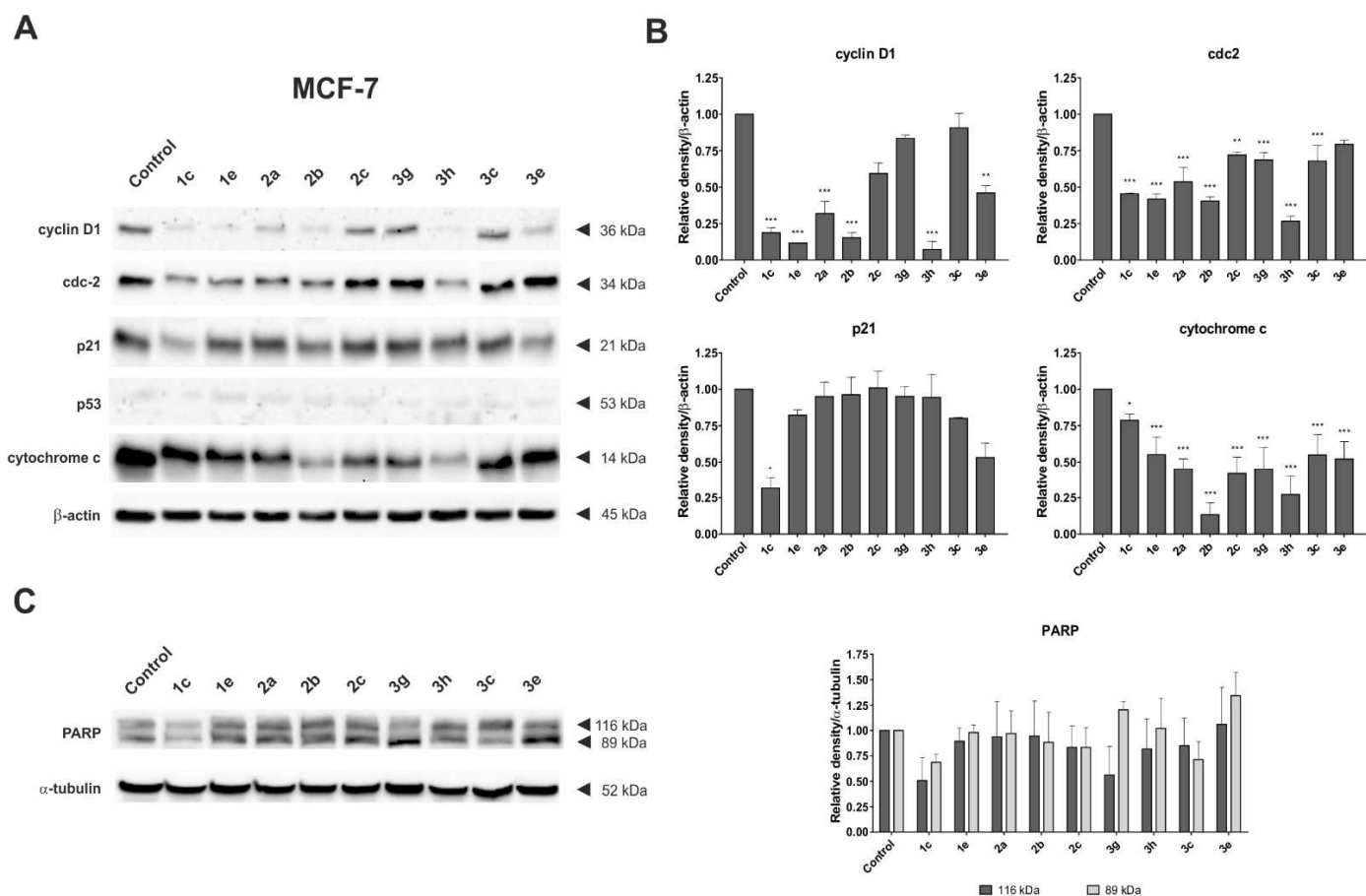


Figure 5: Effect of the tested TSC (concentration $4 \times IC_{50}$) on the expression of cyclin D1, cdc2, p21, p53 and cytochrome c in the MCF-7 cells (A). The densitometric analyses of these proteins were normalized to β -actin. The results are the mean \pm SD of five independent experiments. Statistical differences were analyzed using one-way ANOVA with a Bonferroni's post-hoc test: * $p < 0.05$, ** $p < 0.01$, *** $p < 0.001$ compared to the control group (B). The effect of the TSCs on the cleaving of the PARP protein in MCF-7 cells. The densitometric analysis of PARP was normalized to α -tubulin (C).

From the biochemical point of view, metal chelators deprive cells of intracellular iron, and thereby, disrupt the iron metabolism, which may have an effect on multiple target molecules that are critical in regulating the progression of the cell cycle, cyclins, cyclin-dependent kinases (CDKs), p53 and p21^{CIP/WAF1} (Fig. 4, 5). The progression of the cell cycle in the G1 phase, which is followed by a transition to the S phase, is partially controlled by the activation of the cyclin D1/cdk4 and cyclin E/cdk2 complexes. In addition, the activity of cyclin D1 is associated with the p21^{CIP/WAF1} protein, which plays a crucial role in triggering various effects on the cell cycle regulation. A decrease in the p21^{CIP/WAF1} expression may lead

to the arrest of the G1/S phase cell cycle, thereby affecting the stabilization of the cyclin D1 complex/cdk4. However, on the other hand, by binding iron from the intracellular space, iron chelators may increase the expression of the p21^{CIP/WAF1} protein, which leads to the activation of apoptosis signaling pathways [39]. The S phase in the cell cycle is regulated by cyclin A and its corresponding cdk. In turn, the cdc2 protein, which is the catalytic subunit of the heterodimer with cyclin B, is responsible for the transition to the G2/M phase of the cell cycle. Interestingly, iron chelators cause a marked decrease in cyclin D1, D2 and D3, which causes the expression of cyclins A and B to also be reduced, but to a lesser extent [17]. This supports our observation that all of the tested compounds caused cell cycle arrest in the S and G2/M phases (**Fig. 2, S1, S2**). The same phenomenon has also been reported elsewhere [7]. The most important regulator of the cell cycle is p53, which is involved in both the G1/S and the G2/M checkpoints. p53 is engaged in the response to iron depletion, cellular stress, DNA-damage or the failure of the checkpoints due to the activation of the transcription of many of the genes that are involved in the arrest of growth, DNA repair and apoptosis when the damage is irreversible. Several reports have indicated that DFO may up-regulate the p53 expression at the post-transcriptional stage [40]. Another quinoline-related chelator, COTI-2, has been reported to have a submicromolar activity against cancer cells with p53 mutations [29]. It is able to bind incorrectly folded p53 proteins, thereby promoting its repair and reactivation [41]. Interestingly, the restoration of the tumor-suppressor protein leads to a higher activity (lower IC₅₀) against mutated cells than against their wild-type counterparts [28]. On the other hand, the ability to reactivate p53 does not necessarily mean a high level of activity against mutants with a severely damaged gene or on with deletions [42]. It is noteworthy that HIF1- α is also believed to stabilize p53 and to lead to its up-regulation after iron depletion [43]. However, in our current experiments, no activation of p53 was observed in either of the cell lines that were tested (**Fig. 4, 5**). This, along with the results of the Annexin V binding assay suggests a p53-independent mechanism of action (**Fig. 3, S3, S4**).

The results for the cells that had been incubated with the tested compounds differed for HCT 116 p53^{+/+} and MCF-7. Quite a high basal level of the p21 was detected (in the control cells) for the breast cancer and no overexpression was observed (**Fig. 5**). This result is in accordance with a previously published report on the p21 level in estrogen receptor positive breast cancers [44]. However, the **1c** and **3e** derivatives decreased the level of the p21 protein to 30 and 50%, respectively (**Fig. 5B**). There was a significant overexpression of this protein for all of the tested compounds except **3c** for colon cancer (**Fig. 4B**). The highest effect was observed for the **3g** derivative, in which the p21 level was elevated 4.5-fold. Compounds **1c**,

2a and **2c** also had a strong effect on the p21 level and increased it roughly three-fold. On the other hand, **3h** and **1e** had only a limited effect. Apparently, there was no relationship between the activity level and an increase in the p21 expression. The variation in the reactions to TSC between the cell lines provides insight into the diversity in the regulation mechanisms for the cell cycle. The basal level of the regulatory proteins and its connection with other factors such as hormonal activation constitute a cell's response to changes in the redox equilibrium. In this regard, the absolute level of p21 does not reflect either cell proliferation or a vulnerability to cytostatic agents. Iron chelators such as DFO and **Dp44mT** may increase the level of the p21 protein *via* transcriptional factors as was mentioned earlier. However, the contrary was observed in the case of MCF-7 [45]. Nevertheless, the changes in the p21 protein expression could be a sign of the downstream activation of the apoptotic pathway. Flow cytometry experiments indicated that the population of apoptotic cells was higher among the HCT 116 cells for all of the derivatives (**Fig. 3**).

Another indicator of apoptosis is the release of cytochrome c. In the experiments that were performed, we observed a decrease in the mitochondrial cytochrome c level in both cell lines. The exceptions were **1c**, **3h**, and **3c** in the HCT 116 cells (**Fig 4B**). The highest level of release was observed in the MCF-7 cell line for **2b** (90%), **3h** (70%), **2c**, **3g** and **2a** (60%), **3e**, **1e** and **3c** (50%) (**Fig 5B**). In HCT 116, this down expression was observed to a lesser extent, but for **2c** and **2a** (70%), **2b** (60%), **3e** and **1e** (50%), it was still marked. The last target connected with apoptotic cell dead was the PARP protein. Evidence of apoptotic scenarios is the detection of a cleaved fragment of the PARP protein with molecular mass 89 kDa. We observed cleaved PARP only in the MCF-7 cell for **3e** and **3g** and a small concentration for **3h** (**Fig. 5C**).

These results prompted us to explore two other proteins that are connected with cell cycle regulation – cdc2 and cyclin D1. In general, we observed a decrease in the expression of the cdc2 protein in both of the tested cell lines, except for compounds **3c**, **2b**, **1e** and **1c** on HCT 116. For MCF-7, this downregulation was observed for all of the tested compounds, especially for **3h**, **2b**, **1e**, **1c** and **2a**. It is interesting that the strongest effect for both cell lines was observed for **3h** (70% for HCT 116 and MCF-7). A similar situation was observed for the protein cyclin D1 where there was also a decrease for both of the investigated cell lines except for compounds **2c**, **3h** and **3g** on HCT 116. For MCF-7, this downregulation was particularly strong for **3h**, **1e** and **2b** (90%), **1c** (80%) and **2a** (70%). The same was observed for HCT 116 – **3c**, **3e** and **2b** (90%), **1c** (80%) and **1e** (70%). The most significant difference in the activation and deactivation of the tested proteins was observed for **3h** (downregulation for

MCF-7, upregulation for HCT 116) and **3c** and **3e** (downregulation for HCT 116, upregulation for MCF-7). In general, these results correlate with the cell cycle analysis and confirm the inhibitory effect of the tested compounds on the cell cycle.

2.6. Generation of ROS

TSC are known for their ability to generate ROS in a Fenton and Haber-Weiss reaction and this is undoubtedly an important aspect of the cytotoxicity of TSC. The signaling nature of ROS should be stressed, particularly in cancer cells that have altered redox homeostasis [7]. An increased level of reactive oxygen species can affect many processes such as RR inhibition, which is responsible for catalyzing the synthesis of the deoxyribonucleotides (dNTPs) that are required for DNA synthesis. The activity of RR is determined by subunit R2, which contains a di-nuclear iron center that is responsible for generating and maintaining a tyrosyl radical that is required for catalysis. Its destabilization, which is induced by the generation of ROS by chelators, causes a loss of RR activity and affects the progression of the cell cycle and cell repair [46]. A combination of redox activity and intercalation is a prerequisite for the accumulation of DNA damage. ROS are able to induce single lesions on every base. Changes in the oxidative state have an impact on the progression of the cell cycle through MnSOD and cdc2 [47]. In our study, the ROS level was quantitatively measured in both cell lines according to the CellROX protocol (**Fig. 6**).

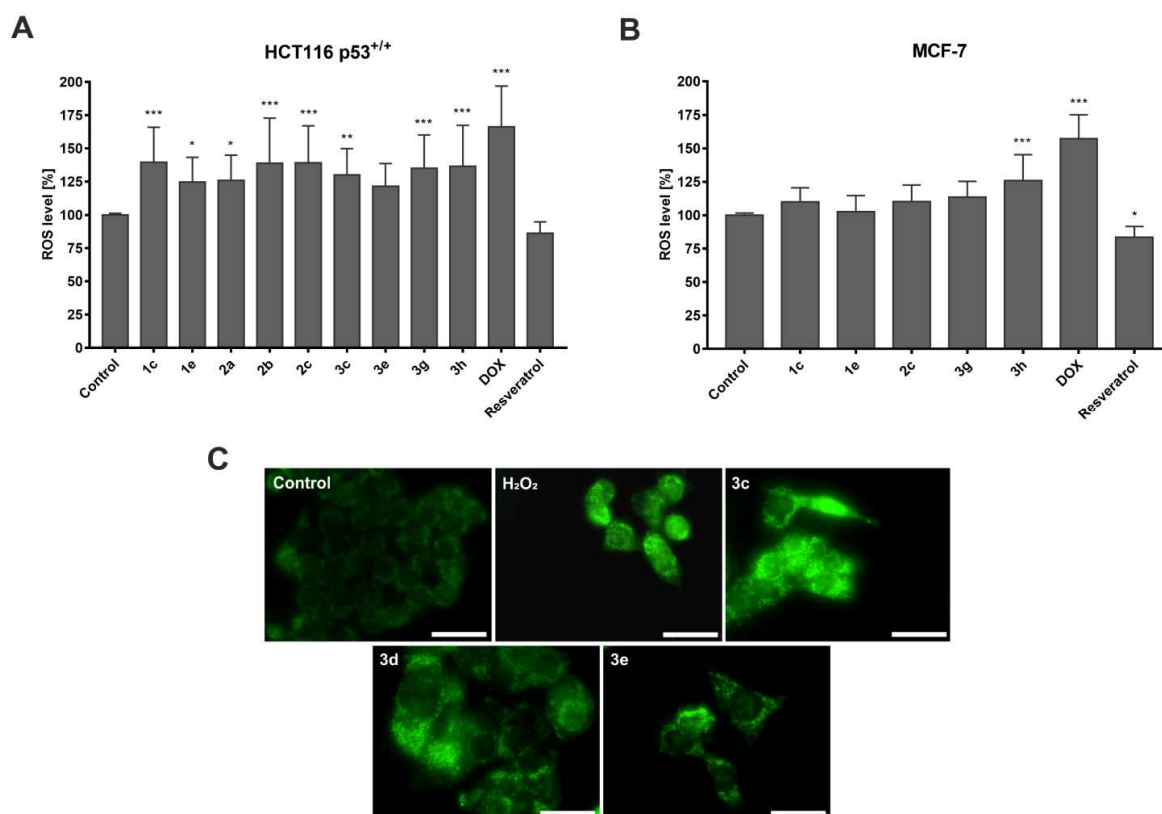


Figure 6: Quantitative measurement of the intracellular ROS level in HCT 116 p53^{+/+} (A) and MCF-7 (B) after a 24-h incubation with the tested TSC (1 μ M), DOX (5 μ M) and antioxidant – resveratrol (100 μ M). The data were normalized to the untreated cells (control). The results are shown as the mean \pm SD of three independent measurements. The data were analyzed using one-way ANOVA with a Bonferroni's post-hoc test: *p < 0.05, ** p < 0.01, *** p < 0.001 compared to the control group. Microscopic images of the formation of ROS in the HCT 116 p53^{+/+} cells after a 24-h treatment with the tested TSC (concentration 2 \times IC₅₀) and a 15-min incubation with hydrogen peroxide (100 μ M). The negative control consisted of untreated cells. Scale bars = 20 μ m (C).

Doxorubicin and resveratrol were used as the positive and negative controls, respectively. In the colon carcinoma, the effect of TSC on the generation of ROS was much higher than in the case of MCF-7. In general, all of the TSC that were tested had a positive response to the ROS level. The strongest effects were observed in for compounds **1c**, **2b**, **2c**, **3g** and **3h**, which correlates with the activities that are presented in **Table 1**. In an analogous experiment that was performed on MCF-7, only **3h** was able to generate ROS to a significant level. A possible explanation might be the fact that MCF-7 has an elevated basal level of ROS and a higher amount of the main GSH antioxidant [48]. It is worth mentioning that colon and breast

cancers have a different pattern of ROS, e.g. breast cancers have a higher superoxide radical but no hydroxyl radical or hypochloric acid [49]. These differences are explained in part by the estrogen-related redox cycle [50]. Noticeably, in our experiments, the resveratrol, which a natural antioxidant, had slightly stronger effect on the MCF-7 than HCT 116 cells.

To confirm the importance of metal chelation in ROS production, we performed experiments in which the metal ions Cu^{2+} and Fe^{3+} were added. As is shown in **Figure S6** there was no significant difference in the activity of TSC alone or after the addition of Fe^{3+} . In some cases (**1e** and **3c**) we even observed a slight decrease in the activity. Iron ions must be reduced to Fe^{2+} in order to participate in the Fenton reaction [51]. However, in most cases, the addition of Cu^{2+} resulted in a substantial improvement of the activity of TSC alone. This synergistic effect is a commonly known fact [7][15] and the explanation is the participation of Cu^{2+} complexes in the Haber-Weiss reaction [11], the great ability of copper to form complexes with TSC [15] and the ionophoric action of TSC, which increases the concentration of copper in the cells [52]. Although the concentration of both metals are tightly regulated in the cell, there are no free copper ions. On the other hand, the storage capacity for this metal is also lower as requirement for this element is well fulfilled by diet [53]. Finally, an internalization of copper to lysosomes has been demonstrated by Stacy et al. as main aspect of overcoming Pgp-mediated drug resistance [35]. For these reasons the addition of Cu^{2+} may result in a stronger decrease of the viability of cells.

Additionally we conducted experiments by adding the non-specific chelator EDTA and we did not observe any significant effect on the cellular proliferation (**Fig. S6**). TSC are particularly strong chelators with high affinity to the iron. According to Bernhardt and coworkers the pyridine based thiosemicarbazones were sufficient to abstract Fe^{3+} from EDTA and DFO complexes in a biologically relevant pH [54]. In our experiment addition of EDTA in the concentration 10 times higher than TSC, has no effect on its activity.

2.7. Intercalation

Higher activity against the p53 mutant and, in particular, the null cell lines may be connected with intercalation or other damage in DNA [42]. TSC may also increase the small changes in genome by forming ROS after binding to DNA [7]. To explore this possibility, a spectroscopic analysis of a mixture of calf-thymus DNA with all of the derivatives was performed. The results are shown in **Table 2** along with doxorubicin, which is well-known strong intercalator [55]. All of the compounds were able to reduce the absorbance of DNA as expected. This effect was particularly strong in **2c** and **3g-3i** and was comparable to the

doxorubicin. Compounds **3h** and **3i** were responsible for a strong redshift in the absorption maxima. The other TSC expressed a moderate but still significant effect with the exception of **3c** and **3e** where the effect was too small for the intercalators. The same has been observed for **Dp44mT**, which is in good agreement with the literature [7]. Interestingly, compound **3c**, which showed no sign of intercalation, also had no selectivity in either of the HCT 116 lines. Hypochromism is considered to be the result of an interaction between the electronic state of chelator and the base pairs in DNA, which is a sign of intercalation. Hyperchromism is more often the effect of a partial uncoiling or groove binding. The absorption spectra of the tested thiosemicarbazones and CT-DNA are presented in **Fig. S7** (Supporting Information).

Table 2: Spectroscopic properties of the tested TSCs that bound to the calf-thymus DNA.

Compound	Absorption	Changes in absorbance	% hypochromism	$\Delta\epsilon \text{ M}^{-1} \text{ cm}^{-1}$	Blue/red shift*
1c	268; 326	hypochromism	15.2	1215.6	8
1e	292	hypochromism	10.3	1606.7	10
2b	310	hypochromism	11.0	935.6	8
2c	396	hypochromism	24.7	955.6	4
3c	262; 300	hypochromism	3.7	1026.7	2
3e	380	hypochromism	5.8	737.8	2
3g	264; 308	hypochromism	25.9	4031.1	2
3h	310	hypochromism	28.7	3155.6	16
3i	364	hypochromism	29.6	6433.3	14
Dp44mT	272; 324	hypochromism	8.2	1673.3	2
Doxorubicin	480	hypochromism	34.2	3235.6	10

*for the wavelengths of maximum absorption for individual and DNA-bound compounds.

3. Conclusions

Based on our results, it is evident that specific cellular regulatory mechanisms are crucial for understanding the antiproliferative activity of TSC. For example, the alternative regulation of the pro- and anti-apoptotic proteins may determine the intrinsic reaction of a cell to an active dose of a chelator. On the other hand, however, the chemical structure determines the additional features such as DNA intercalation, ROS generation or ionophoric activity. These, in turn, may result in the selectivity profile of a drug. In this regard, more data would be valuable in designing iron chelators for the specific biochemical microenvironment that TSC deal with.

4. Experimental session

4.1. Chemistry

4.1.1. General

Microwave reactions were carried out in a Discover® BenchMate™ (CEM) microwave equipped with 10 mL vessels. Melting point measurements were determined in a Stanford Research Systems OptiMelt (MPA 100). The ^1H and ^{13}C NMR spectra were recorded on a Bruker Ascend 500 MHz spectrometer at frequencies of 500 MHz and 126 MHz and a Bruker Avance III 400 MHz FT-NMR spectrometer at frequencies of 400 MHz and 101 MHz using $\text{DMSO-}d_6$ as the solvent and TMS as the internal standard. The NMR solvents were purchased from ACROS Organics. The chemical shifts (δ) are given in ppm and the coupling constants (J) values are reported in hertz (Hz). The spin multiplicities are described as s (singlet), d (doublet), dd (double of doublets), t (triplet), q (quartet) and m (multiplet). The mass spectra were recorded with a Varian 500-MS IT Mass Spectrometer. Elemental analyses (for C, H, N) were carried out on an automatic Perkin-Elmer 240 microanalyzer (Boston, MA, USA) and were within 0.4% of the calculated values. All of the evaporations were performed on a rotary evaporator under diminished pressure at 60°C. All of the reagents and solvents, which were purchased from ACROS Organics, Asta-Tech, Maybridge, Santa Cruz Biotechnology and Sigma-Aldrich, were used without further purification. The purity of the thiosemicarbazones was confirmed by HPLC and was at least 95%.

4.1.2. General procedure for the synthesis of the thiosemicarbazides

The mixtures of (1,1'-thiocarbonyl) bis-1H-imidazole (5 mmol) and suitable derivative of piperazine or thiomorpholine (5 mmol) in methylene chloride (25 ml) were stirred for 24 h at room temperature. The solutions were extracted three times with distilled water and the organic phases were dried over MgSO_4 and evaporated. The obtained thioketones were refluxed for 2 hours with hydrazine hydrate (5 mmol). The final thiosemicarbazides were crystallized from dry methanol.

Thiomorpholine-4-carbothiohydrazide - precursor of 1b and 3a

White crystal powder; yield 89%; mp: 160-161 °C; $^1\text{H-NMR}$ (400 MHz, d_6 -DMSO, ppm): δ 4.03 (m, 8H, CH_2), 4.83 (s, 2H, NH_2), 9.19 (s, 1H, NH). $^{13}\text{C-NMR}$ (101 MHz, d_6 -DMSO, ppm): δ 26.4; 50.8; 182.3.

4-(3,4-dichlorophenyl)piperazine-1-carbothiohydrazide - precursor of 1c, 3c and 3i

White powder; yield 68%; mp: 186-187 °C; ¹H-NMR (400 MHz, *d*₆-DMSO, ppm): δ 3.08 (s, 4H, CH₂), 3.86 (m, 4H, CH₂), 4.76 (s, 2H, NH₂), 6.93 (m, 1H, Ar-H), 7.14 (s, 1H, Ar-H), 7.40 (d, 1H, *J* = 9.0 Hz), 9.19 (s, 1H, NH). ¹³C-NMR (101 MHz, *d*₆-DMSO, ppm): δ 47.1; 47.3; 115.6; 116.6; 120.1; 130.9; 132.0; 150.7; 183.0.

4-(4-nitrophenyl)piperazine-1-carbothiohydrazide - precursor of 1d, 2c, 3e and 3f

Yellow powder; yield 87%; mp: 207-208 °C; ¹H-NMR (400 MHz, *d*₆-DMSO, ppm): δ 3.57 (s, 4H, CH₂), 3.91 (s, 4H, CH₂), 4.97 (s, 2H, NH₂), 6.97 (d, 2H, *J* = 9.3 Hz), 8.08 (m, 2H, Ar-H), 9.15 (s, 1H, NH). ¹³C-NMR (101 MHz, *d*₆-DMSO, ppm): δ 45.7; 46.7; 112.5; 126.2; 137.3; 154.6; 182.8.

4-(4-cyanophenyl)piperazine-1-carbothiohydrazide - precursor of 1e and 3b

Light orange powder; yield 70%; mp: 169-170 °C; ¹H-NMR (400 MHz, *d*₆-DMSO, ppm): δ 3.42 (m, 4H, CH₂), 3.89 (m, 4H, CH₂), 4.78 (s, 2H, NH₂), 7.05 (s, 2H, Ar-H), 7.60 (m, 2H, Ar-H), 9.15 (s, 1H, NH). ¹³C-NMR (101 MHz, *d*₆-DMSO, ppm): δ 45.9; 48.9; 98.6; 114.3; 120.5; 133.8; 153.0; 182.9.

4-(4-methoxyphenyl)piperazine-1-carbothiohydrazide - precursor of 2a, 3d and 3j

White powder; yield 81%; mp: 194-195 °C; ¹H-NMR (400 MHz, *d*₆-DMSO, ppm): δ 3.00 (s, 3H, CH₃), 3.86 (m, 4H, CH₂), 4.11 (m, 4H, CH₂), 4.77 (s, 2H, NH₂), 6.83 (d, 2H, *J* = 9.0 Hz), 6.90 (m, 2H, Ar-H), 9.17 (s, 1H, NH). ¹³C-NMR (101 MHz, *d*₆-DMSO, ppm): δ 19.0; 49.9; 56.5; 114.8; 118.2; 145.4; 153.7; 183.1.

4-(4-fluorophenyl)piperazine-1-carbothiohydrazide - precursor of 2b

Light pink powder; yield 97%; mp: 180-181 °C; ¹H-NMR (400 MHz, *d*₆-DMSO, ppm): δ 3.09 (m, 4H, CH₂), 3.87 (m, 4H, CH₂), 4.77 (s, 2H, NH₂), 6.97 (m, 2H, Ar-H), 7.05 (m, 2H, Ar-H), 9.19 (s, 1H, NH). ¹³C-NMR (101 MHz, *d*₆-DMSO, ppm): δ 47.6; 49.1; 115.9; 117.9; 148.0; 157.8; 183.0.

4-[4-(trifluoromethyl)phenyl]piperazine-1-carbothiohydrazide precursor of 3g

White powder; yield 56%; mp: 181-182 °C; ¹H-NMR (400 MHz, *d*₆-DMSO, ppm): δ 3.18 (m, 4H, CH₂), 3.90 (s, 4H, CH₂), 4.77 (s, 2H, NH₂), 7.07 (s, 2H, Ar-H), 7.51 (d, 2H, *J* = 8.4 Hz),

9.18 (s, 1H, NH). ¹³C-NMR (101 MHz, *d*₆-DMSO, ppm): δ 46.6; 47.1; 114.3; 118.1; 118.4; 126.7; 153.2; 183.0.

4-[5-(trifluoromethyl)pyridin-2-yl]piperazine-1-carbothiohydrazide precursor of 3h

White powder; yield 70%; mp: 206-207 °C; ¹H-NMR (400 MHz, *d*₆-DMSO, ppm): δ 3.70 (s, 4H, CH₂), 3.87 (s, 4H, CH₂), 4.76 (s, 2H, NH₂), 6.93 (d, 1H, *J* = 9.1 Hz), 7.82 (s, 1H, Ar-H), 8.42 (s, 1H, Ar-H), 9.14 (s, 1H, NH). ¹³C-NMR (101 MHz, *d*₆-DMSO, ppm): δ 43.8; 46.9; 49.1; 106.7; 113.7; 135.0; 145.7; 160.3; 183.0.

4.1.3. General procedure for synthesizing the thiosemicarbazones

Two drops of glacial acetic acid as a catalyst were added to the mixtures of thiosemicarbazides (0.5 mmol) and di(2-pyridyl) ketone, 2-pyridinecarboxaldehyde, 2-quinolinecarboxaldehyde, 8-hydroxy-2-quinolinecarboxaldehyde or 2-quinolinecarbaldehyde (0.5 mmol) in ethanol (5 ml). The glass tubes were sealed and placed into a microwave reactor at 83 °C for 20 minutes (the reactor power did not exceed 50W). The final products were crystallized from dry methanol.

N'-[di(pyridin-2-yl)methylidene]-4-thiomorpholine-1-carbothiohydrazide (**1b**)

Yellow powder; yield 86%; mp: 223-224 °C; ¹H-NMR (400 MHz, *d*₆-DMSO, ppm): δ 2.78 (s, 4H, CH₂), 4.28 (s, 4H, CH₂), 7.53 (m, 3H, Ar-H), 7.96 (m, 3H, Ar-H), 8.59 (m, 1H, Ar-H), 8.82 (m, 1H, Ar-H), 14.65 (s, 1H, NH). ¹³C-NMR (126 MHz, *d*₆-DMSO, ppm): δ 51.9; 56.5; 123.6; 124.3; 126.3; 137.5; 148.6; 148.9; 156.0. HRMS (ESI): *m/z* calculated for C₁₆H₁₈N₅S₂: 344.1004, found: 344.1004 [M+H]⁺.

N'-[di(pyridin-2-yl)methylidene]-4-(3,4-dichlorophenyl)piperazine-1-carbothiohydrazide (**1c**)

Yellow powder; yield 48%; mp: 159-160 °C; ¹H-NMR (400 MHz, *d*₆-DMSO, ppm): δ 3.46 (s, 4H, CH₂), 4.15 (s, 4H, CH₂), 7.13 (d, 1H, *J* = 2.6 Hz), 7.43 (d, 1H, *J* = 9.0 Hz), 7.49 (m, 1H, Ar-H), 7.61 (m, 2H, Ar-H), 7.98 (m, 4H, Ar-H), 8.61 (d, 1H, *J* = 3.9 Hz), 8.88 (d, 1H, *J* = 4.2 Hz), 14.66 (s, 1H, NH). ¹³C-NMR (126 MHz, *d*₆-DMSO, ppm): δ 47.0; 48.9; 115.2; 116.2; 119.8; 124.2; 125.1; 127.4; 131.0; 132.1; 137.8; 149.1; 150.3; 156.0; 180.6. HRMS (ESI): *m/z* calculated for C₂₂H₂₁Cl₂N₆S: 471.0925, found: 471.0934 [M+H]⁺.

N'-[di(pyridin-2-yl)methylidene]-4-(4-nitrophenyl)piperazine-1-carbothiohydrazide (**1d**)

Yellow powder; yield 44%; mp: 194-195 °C; ¹H-NMR (400 MHz, *d*₆-DMSO, ppm): δ 3.84 (m,

4H, CH₂), 4.82 (m, 4H, CH₂), 6.97 (s, 3H, Ar-H), 7.55 (d, 2H, *J* = 4.2 Hz), 8.07 (s, 3H, Ar-H), 8.52 (s, 2H, Ar-H), 8.83 (s, 1H, Ar-H), 9.15 (s, 1H, Ar-H), 14.67 (s, 1H, NH). ¹³C-NMR (126 MHz, *d*₆-DMSO, ppm): δ 45.8; 48.5; 112.3; 113.6; 120.2; 124.2; 126.3; 129.8; 136.9; 148.7; 148.9; 154.6; 182.8. HRMS (ESI): *m/z* calculated for C₂₂H₂₂N₇O₂S: 448.1556, found: 448.1550 [M+H]⁺.

N'-[di(pyridin-2-yl)methylidene]-4-(4-cyanophenyl)piperazine-1-carbothiohydrazide (**1e**)

Light orange powder; yield 33%; mp: 186-187 °C; ¹H-NMR (400 MHz, *d*₆-DMSO, ppm): δ 3.58 (s, 4H, CH₂), 4.32 (s, 4H, CH₂), 6.84 (d, 2H, *J* = 8.7 Hz), 7.28 (s, 1H, Ar-H), 7.41 (m, 2H, Ar-H), 7.54 (d, 3H, *J* = 8.7 Hz), 7.87 (m, 2H, Ar-H), 8.66 (d, 1H, *J* = 3.5 Hz), 8.78 (d, 1H, *J* = 3.8 Hz), 14.83 (s, 1H, NH). ¹³C-NMR (126 MHz, *d*₆-DMSO, ppm): δ 46.1; 48.7; 99.3; 113.6; 114.9; 120.4; 124.3; 127.3; 133.9; 137.8; 148.9; 153.3; 156.0; 180.5. HRMS (ESI): *m/z* calculated for C₂₃H₂₂N₇S: 428.1657, found: 428.1648 [M+H]⁺.

4-(4-methoxyphenyl)-*N'*-[(pyridin-2-yl)methylidene]piperazine-1-carbothiohydrazide (**2a**)

Brown powder; yield 36%; mp: 161-162 °C; ¹H-NMR (400 MHz, *d*₆-DMSO, ppm): δ 2.72 (m, 4H, CH₂), 3.17 (s, 3H, CH₃), 3.68 (m, 4H, CH₂), 6.84 (s, 2H, Ar-H), 7.31 (m, 1H, Ar-H), 7.40 (m, 1H, Ar-H), 7.55 (m, 1H, Ar-H), 7.67 (m, 1H, Ar-H), 7.84 (m, 1H, Ar-H), 8.55 (d, 1H, *J* = 4.3 Hz), 10.37 (s, 1H, CH), 15.24 (s, 1H, NH). ¹³C-NMR (101 MHz, *d*₆-DMSO, ppm): δ 49.7; 55.6; 114.8; 118.2; 123.0; 125.1; 137.1; 145.2; 148.2; 149.5; 153.8; 156.8; 170.8; 182.3. HRMS (ESI): *m/z* calculated for C₁₈H₂₂N₅OS: 356.1545, found: 356.1545 [M+H]⁺.

4-(4-fluorophenyl)-*N'*-[(pyridin-2-yl)methylidene]piperazine-1-carbothiohydrazide (**2b**)

Light brown powder; yield 43%; mp: 162-163 °C; ¹H-NMR (400 MHz, *d*₆-DMSO, ppm): δ 3.17 (s, 4H, CH₂), 4.11 (m, 4H, CH₂), 7.00 (m, 2H, Ar-H), 7.08 (m, 2H, Ar-H), 7.86 (m, 2H, Ar-H), 8.21 (s, 1H, Ar-H), 8.57 (dd, 1H, *J* = 11.3; 4.7 Hz), 11.48 (s, 1H, CH), 15.24 (s, 1H, NH). ¹³C-NMR (101 MHz, *d*₆-DMSO, ppm): δ 49.0; 49.4 (d *J* = 6.2 Hz); 50.3; 115.7; 117.9 (dd, *J* = 13.3, 7.6 Hz); 120.0; 124.5; 137.3; 144.6; 147.9; 149.9; 153.8; 181.2. HRMS (ESI): *m/z* calculated for C₁₇H₁₉FN₅S: 344.1345, found: 344.1341 [M+H]⁺.

4-(4-nitrophenyl)-*N'*-[(pyridin-2-yl)methylidene]piperazine-1-carbothiohydrazide (**2c**)

Yellow powder; yield 73%; mp: 213-214 °C; ¹H-NMR (400 MHz, *d*₆-DMSO, ppm): δ 3.69 (s, 4H, CH₂), 4.13 (s, 4H, CH₂), 6.97 (t, 2H, *J* = 8.2 Hz), 7.39 (m, 1H, Ar-H), 7.87 (m, 1H, Ar-H), 8.10 (d, 2H, *J* = 9.1 Hz), 8.22 (s, 1H, Ar-H), 8.59 (d, 1H, *J* = 4.3 Hz), 11.52 (s, 1H, CH),

15.19 (s, 1H, NH). $^{13}\text{C-NMR}$ (126 MHz, d_6 -DMSO, ppm): δ 45.8; 49.4; 112.5; 120.1; 124.6; 126.3; 137.2; 137.3; 144.6; 150.0; 153.8; 154.5; 181.1. HRMS (ESI): m/z calculated for $\text{C}_{17}\text{H}_{19}\text{N}_6\text{O}_2\text{S}$: 371.1290, found: 371.1280 $[\text{M}+\text{H}]^+$.

N'-[(quinolin-2-yl)methylidene]-4-thiomorpholine-1-carbothiohydrazide (3a)

Yellow powder; yield 34%; mp: 198-199 °C; $^1\text{H-NMR}$ (400 MHz, d_6 -DMSO, ppm): δ 2.71 (s, 4H, CH_2), 3.71 (s, 4H, CH_2), 7.61 (d, 1H, $J = 6.5$ Hz), 7.76 (d, 1H, $J = 7.1$ Hz), 7.97 (dd, 3H, $J = 15.1$; 7.9 Hz), 8.14 (s, 1H, Ar-H), 8.35 (s, 1H, CH), 12.32 (s, 1H, NH). $^{13}\text{C-NMR}$ (126 MHz, d_6 -DMSO, ppm): δ 25.7; 52.1; 117.4; 127.3; 128.0; 128.4; 129.2; 130.5; 136.9; 142.4; 147.9; 154.2; 163.2. HRMS (ESI): m/z calculated for $\text{C}_{15}\text{H}_{17}\text{N}_4\text{S}_2$: 317.0895, found: 317.0895 $[\text{M}+\text{H}]^+$.

4-(4-cyanophenyl)-N'-[(quinolin-2-yl)methylidene]piperazine-1-carbothiohydrazide (3b)

Yellow powder; yield 70%; mp: 202-203 °C; $^1\text{H-NMR}$ (400 MHz, d_6 -DMSO, ppm): δ 3.58 (s, 4H, CH_2), 4.14 (s, 4H, CH_2), 7.02 (d, 3H, $J = 8.5$ Hz), 7.09 (d, 1H, $J = 8.5$ Hz), 7.64 (m, 2H, Ar-H), 7.81 (m, 2H, Ar-H), 8.03 (m, 2H, Ar-H), 8.37 (s, 1H, CH), 11.67 (s, 1H, NH). $^{13}\text{C-NMR}$ (126 MHz, d_6 -DMSO, ppm): δ 45.8; 49.4; 98.5; 114.1; 114.8; 117.8; 120.4; 128.4; 129.3; 130.4; 133.8; 137.0; 144.0; 148.0; 153.0; 153.9; 173.0; 181.2. HRMS (ESI): m/z calculated for $\text{C}_{22}\text{H}_{21}\text{N}_6\text{S}$: 401.1548, found: 401.1555 $[\text{M}+\text{H}]^+$.

4-(3,4-dichlorophenyl)-N'-[(quinolin-2-yl)methylidene]piperazine-1-carbothiohydrazide (3c)

Yellow powder; yield 77%; mp: 188-189 °C; $^1\text{H-NMR}$ (400 MHz, d_6 -DMSO, ppm): δ 3.41 (s, 4H, CH_2), 4.12 (s, 4H, CH_2), 6.97 (d, 1H, $J = 8.8$ Hz), 7.18 (s, 1H, Ar-H), 7.44 (d, 1H, $J = 8.9$ Hz), 7.63 (t, 1H, $J = 7.3$ Hz), 7.79 (t, 1H, $J = 7.6$ Hz), 8.02 (m, 3H, Ar-H), 8.35 (s, 1H, CH), 8.39 (d, 1H, $J = 8.6$ Hz), 11.67 (s, 1H, NH). $^{13}\text{C-NMR}$ (126 MHz, d_6 -DMSO, ppm): δ 47.6; 50.0; 115.5; 116.5; 117.8; 120.1; 127.7; 128.2; 128.5; 129.3; 130.6; 131.0; 132.0; 137.2; 144.4; 147.9; 150.6; 154.3; 181.2. HRMS (ESI): m/z calculated for $\text{C}_{21}\text{H}_{20}\text{Cl}_2\text{N}_5\text{S}$: 444.0816, found: 444.0810 $[\text{M}+\text{H}]^+$.

4-(4-methoxyphenyl)-N'-[(quinolin-2-yl)methylidene]piperazine-1-carbothiohydrazide (3d)

Yellow powder; yield 78%; mp: 161-162 °C; $^1\text{H-NMR}$ (400 MHz, d_6 -DMSO, ppm): δ 3.17 (m, 4H, CH_2), 3.70 (m, 3H, CH_3), 4.12 (m, 4H, CH_2), 6.86 (d, 2H, $J = 9.1$ Hz), 6.96 (d, 2H, $J = 9.1$ Hz), 7.63 (m, 1H, Ar-H), 7.79 (m, 1H, Ar-H), 7.99 (m, 1H, Ar-H), 8.03 (m, 2H, Ar-H), 8.34 (s, 1H, CH), 8.39 (d, 1H, $J = 8.7$ Hz), 11.65 (s, 1H, NH). $^{13}\text{C-NMR}$ (126 MHz, d_6 -

DMSO, ppm): δ 50.2; 50.5; 55.7; 114.8; 117.7; 118.2; 127.6; 128.2; 128.5; 129.3; 130.5; 137.2; 144.3; 145.4; 147.9; 153.7; 154.3; 181.2. HRMS (ESI): m/z calculated for $C_{22}H_{24}N_5OS$: 406.1702, found: 406.1695 $[M+H]^+$.

4-(4-nitrophenyl)-N'-[(quinolin-2-yl)methylidene]piperazine-1-carbothiohydrazide (3e)

Yellow powder; yield 65%; mp: 206-207 °C; 1H -NMR (400 MHz, d_6 -DMSO, ppm): δ 3.72 (m, 4H, CH₂), 4.17 (m, 4H, CH₂), 7.01 (d, 1H, $J = 8.9$ Hz), 7.63 (m, 1H, Ar-H), 7.79 (m, 1H, Ar-H), 8.01 (m, 2H, Ar-H), 8.05 (d, 2H, $J = 8.7$ Hz), 8.11 (d, 2H, $J = 9.4$ Hz), 8.35 (s, 1H, CH), 8.38 (d, 1H, $J = 8.7$ Hz), 11.70 (s, 1H, NH). ^{13}C -NMR (126 MHz, d_6 -DMSO, ppm): δ 45.8; 49.6; 112.5; 117.9; 126.3; 127.7; 128.2; 128.5; 129.3; 130.5; 137.1; 137.2; 144.4; 147.9; 154.3; 154.5; 181.1. HRMS (ESI): m/z calculated for $C_{21}H_{21}N_6O_2S$: 421.1447, found: 421.1459 $[M+H]^+$.

N'-[(8-hydroxyquinolin-2-yl)methylidene]-4-(4-nitrophenyl)piperazine-1-carbothiohydrazide (3f)

Yellow powder; yield 78%; mp: 204-205 °C; 1H -NMR (400 MHz, d_6 -DMSO, ppm): δ 3.74 (m, 4H, CH₂), 4.14 (m, 4H, CH₂), 6.98 (t, 2H, $J = 10.2$ Hz), 7.12 (m, 2H, Ar-H), 7.42 (m, 2H, Ar-H), 8.08 (m, 2H, Ar-H), 8.29 (d, 1H, $J = 8.7$ Hz), 8.38 (s, 1H, CH), 9.84 (s, 1H, OH), 11.74 (s, 1H, NH). ^{13}C -NMR (126 MHz, d_6 -DMSO, ppm): δ 45.8; 49.6; 112.4; 112.6; 117.8; 118.6; 126.3; 128.6; 129.2; 137.0; 137.3; 138.6; 144.3; 152.2; 153.6; 154.5; 181.0. HRMS (ESI): m/z calculated for $C_{21}H_{21}N_6O_3S$: 437.1396, found: 437.1387 $[M+H]^+$.

4-[(4-trifluoromethyl)phenyl]-N'-[(quinolin-2-yl)methylidene]piperazine-1-carbothiohydrazide (3g)

Yellow powder; yield 83%; mp: 207-208 °C; 1H -NMR (400 MHz, d_6 -DMSO, ppm): δ 3.52 (s, 4H, CH₂), 4.15 (s, 4H, CH₂), 7.09 (d, 2H, $J = 8.0$ Hz), 7.55 (d, 2H, $J = 7.9$ Hz), 7.63 (t, 1H, $J = 7.2$ Hz), 7.79 (t, 1H, $J = 7.1$ Hz), 8.02 (m, 3H, Ar-H), 8.35 (s, 1H, CH), 8.39 (d, 1H, $J = 8.6$ Hz), 11.68 (s, 1H, NH). ^{13}C -NMR (126 MHz, d_6 -DMSO, ppm): δ 46.8; 49.9; 114.3; 117.8; 118.4; 124.4; 126.7 (d, $J = 3.7$ Hz); 127.7; 128.2; 128.5; 129.3; 130.6; 137.2; 144.4; 147.9; 153.1; 154.3; 181.2. HRMS (ESI): m/z calculated for $C_{22}H_{21}F_3N_5S$: 444.1470, found: 444.1473 $[M+H]^+$.

4-[5-(trifluoromethyl)pyridin-2-yl]-N'-[(quinolin-2-yl)methylidene]piperazine-1-carbothiohydrazide (3h)

Yellow crystal powder; yield 68%; mp: 202-203 °C; ¹H-NMR (400 MHz, *d*₆-DMSO, ppm): δ 3.85 (s, 4H, CH₂), 4.13 (s, 4H, CH₂), 6.97 (d, 1H, *J* = 8.9 Hz), 7.63 (t, 1H, *J* = 7.2 Hz), 7.79 (t, 1H, *J* = 7.4 Hz), 7.86 (d, 1H, *J* = 8.6 Hz), 8.02 (m, 3H, Ar-H), 8.35 (s, 1H, CH), 8.38 (m, 1H, Ar-H), 8.46 (s, 1H, Ar-H), 11.67 (s, 1H, NH). ¹³C-NMR (126 MHz, *d*₆-DMSO, ppm): δ 44.1; 49.9; 106.7; 113.8; 114.0; 117.8; 127.6; 128.2; 128.5; 129.3; 130.5; 135.0 (d, *J* = 3.1 Hz); 137.1; 144.4; 145.7(m); 147.9; 154.3; 160.3; 181.4. HRMS (ESI): *m/z* calculated for C₂₁H₂₀F₃N₆S: 445.1422, found: 445.1411 [M+H]⁺.

4-(3,4-dichlorophenyl)-N'-[(quinoxalin-2-yl)methylidene]piperazine-1-carbothiohydrazide
(3i)

Yellow powder; yield 96%; mp: 177-178 °C; ¹H-NMR (400 MHz, *d*₆-DMSO, ppm): δ 3.41 (m, 4H, CH₂), 4.13 (m, 4H, CH₂), 6.96 (m, 1H, Ar-H), 7.17 (d, 1H, *J* = 2.7 Hz), 7.43 (dd, 1H, *J* = 9.0; 2.5 Hz), 7.87 (m, 2H, Ar-H), 8.10 (m, 2H, Ar-H), 8.35 (s, 1H, CH), 9.38 (s, 1H, Ar-H), 11.82 (s, 1H, NH). ¹³C-NMR (126 MHz, *d*₆-DMSO, ppm): δ 47.5; 50.1; 115.5; 116.5; 120.1; 129.5; 130.9; 131.0; 131.2; 132.0; 132.3; 141.8; 141.9; 142.1; 143.3; 149.0; 150.5; 181.1. HRMS (ESI): *m/z* calculated for C₂₀H₁₉Cl₂N₆S: 445.0769, found: 445.0788 [M+H]⁺.

4-(4-methoxyphenyl)-N'-[(quinoxalin-2-yl)methylidene]piperazine-1-carbothiohydrazide **(3j)**

Yellow powder; yield 90%; mp: 162-163 °C; ¹H-NMR (400 MHz, *d*₆-DMSO, ppm): δ 3.18 (m, 4H, CH₂), 3.70 (s, 3H, CH₃), 4.14 (m, 4H, CH₂), 6.86 (m, 2H, Ar-H), 6.97 (m, 2H, Ar-H), 7.87 (m, 2H, Ar-H), 8.10 (m, 2H, Ar-H), 8.35 (s, 1H, CH), 9.37 (s, 1H, Ar-H), 11.78 (s, 1H, NH). ¹³C-NMR (126 MHz, *d*₆-DMSO, ppm): δ 50.2; 50.6; 55.7; 114.8; 118.2; 129.5; 130.9; 131.2; 136.8; 141.8; 141.9; 142.0; 143.3; 145.3; 149.1; 153.8; 181.1. HRMS (ESI): *m/z* calculated for C₂₁H₂₃N₆OS: 407.1654, found: 407.1673 [M+H]⁺.

4.2. Biological assays

4.2.1. Cell culture

The human colon cancer cell line HCT 116 p53^{+/+} and the human breast carcinoma cell line MCF-7 were obtained from ATCC. The HCT 116 that have a p53 deletion (p53^{-/-}) were kindly provided by prof. M. Rusin from the Maria Skłodowska-Curie Memorial Cancer Center and Institute of Oncology in Gliwice, Poland. The glioma cell lines U-251 and Hs 683 were kindly provided by prof. G. Kramer-Marek from The Institute of Cancer Research in London, England. The normal human fibroblast cell lines NHDF were obtained from PromoCell. The cells were grown as monolayer cultures in Dulbecco's modified Eagle's

medium combined with the antibiotics penicillin/streptomycin (Gibco) (1% v/v) in 75 cm² flasks (Nunc). DMEM for HCT 116, MCF-7, U-251 and Hs 683 were supplemented with 12% heat-inactivated fetal bovine serum (Sigma) and for NHDF with 15% non-inactivated fetal bovine serum (Sigma). The cells were cultured under standard conditions at 37°C in a humidified atmosphere at 5% CO₂. All of the cell lines were subjected to routine mycoplasma testing using the PCR technique with specific *Mycoplasma* primers in order to ensure that there was no contamination.

4.2.2. Cytotoxicity studies

The cells were seeded in 96-well plates (Nunc) at a density of 5,000 cells/well (HCT 116, MCF-7, U-251, Hs 683) and 4,000 cells/well (NHDF) and incubated at 37°C for 24 h. The assay was performed following a 72-h incubation with varying concentrations of the compounds that were being tested. Then, 20 µL of the CellTiter 96[®] AQueous One Solution-MTS (Promega) was added to each well (with 100 µL DMEM without phenol red) and incubated for 1 h at 37°C. The optical densities of the samples were analyzed at 490 nm using a multi-plate reader (Synergy 4, Bio Tek). The results are expressed as a percentage of the control and were calculated as the inhibitory concentration (IC₅₀) values (using GraphPad Prism 7). The IC₅₀ parameter was defined as the concentration of a compound that was necessary to reduce the proliferation of cells to 50% of the untreated control. Each individual compound was tested in triplicate in a single experiment with each experiment being repeated three or four times.

4.2.3. Impact of copper and iron ions on cellular proliferation

The HCT 116 cells were seeded in 96-well plates (Nunc) at a density of 5,000 cells/well and incubated at 37°C for 24 h. The next day, freshly prepared solutions of the tested thiosemicarbazone derivatives, **1c**, **1e**, **2a-c**, **3c**, **3e**, **3h**, at varying concentrations were added to the plate and incubated for the next 72h. Additionally, a 20 µM solution of CuSO₄ or FeCl₃, was added into wells with the tested compounds. The controls that were supplemented with these metal solutions did not affect the cell viability (>95 %). An MTS assay was performed as was described above. The results are expressed as a percentage of the control. Each individual compound was tested in triplicate in a single experiment with each experiment being repeated three times.

4.2.4. Effect of an EDTA chelator on cellular proliferation

The HCT 116 cells were seeded in 96-well plates (Nunc) at a density of 5,000 cells/well and incubated at 37°C for 24 h. The next day, freshly prepared solutions of the tested compounds, **1c**, **1e**, **2a-c**, **3c**, **3e**, **3h**, at IC₅₀ concentrations were added to the plate and incubated for the next 72h. Additionally, freshly prepared solutions of EDTA at one, five and ten-fold IC₅₀ concentrations that corresponded to the TSC were added into each well. The controls that were supplemented with EDTA did not affect the cell viability (>95 %). An MTS assay was performed as was described above. The results are expressed as a percentage of the control (untreated cells). Each individual compound was tested in triplicate in a single experiment with each experiment being repeated three times.

4.2.5. Reactive oxygen species formation – microscope images

The HCT 116 p53^{+/+} cells were seeded into eight-well chambers (Lab-Tek) at a density of 0.5·10⁵ cells/well and incubated at 37°C. After 24 h, freshly prepared solutions of the tested compounds, **3c**, **3d**, **3e** (two-fold IC₅₀ concentration), were added. The next day, the solutions of the tested compounds were removed and the cells were washed with Phosphate Buffered Saline (PBS) after which 5 μM of CellROX® Green Reagent (Molecular Probes™) was added. After 30 min of incubation at 37°C, the cells were washed with PBS and then DMEM without phenol red was added. The observation was performed using an inverted fluorescence microscope (IX81, Olympus) that was equipped with a CO₂ incubator using a 485 nm excitation laser and a 520 nm emission filter.

4.2.6. Quantitative measurement of the level of ROS

The HCT 116 p53^{+/+} and MCF-7 cells were seeded onto black 96-well plates (Corning) at a density of 9,000 cells/well and incubated at 37°C. After an overnight incubation, the solutions of the tested compounds, **1c**, **1e**, **2a-c**, **3c**, **3e**, **3g-h** (1 μM) and **DOX** (5 μM), were added and incubated for 24 h. In addition, solutions of 100 μM H₂O₂ (positive control) for 20 min and 100 μM resveratrol (negative control) for 24 h were added to the cells. The generation of ROS was measured using a CellROX® Green Reagent (Molecular Probes™). Additionally, the quantity of cells in each well was determined using Hoechst 33342 (Molecular Probes™). The solutions of the tested compounds were removed and 100 μL of CellROX Green Reagent and Hoechst 33342 at a final concentration of 5 μM were added to each well. Then, the cells were incubated for 30 min at 37°C. The fluorescence was measured using a multi-plate reader (Synergy 4, Bio Tek) at a 485 nm excitation and a 520 nm emission for the CellROX Green Reagent and a 345 nm excitation laser and a 485 nm

emission filter for Hoechst 33342. The experiments were performed three to four times. The levels of ROS are expressed as the percentage of the level of the control cells.

4.2.7. Immunoblotting

The HCT 116 p53^{+/+} and MCF-7 cells were seeded in 3 cm Petri dishes (Nunc) at a density of $0.5 \cdot 10^6$ cells/well and incubated overnight. The next day, solutions of **1c**, **1e**, **2a-c**, **3c**, **3e**, **3g-h** (four-fold IC₅₀ concentration) were added and the cells were incubated for 24 h. Cells were harvested using trypsinization and washed with cold PBS. Next, the cells were centrifuged and suspended in an RIPA buffer (Thermo Scientific) containing a Halt Protease Inhibitor Cocktail (Thermo Scientific) and a Halt Phosphatase Inhibitor Cocktail (Thermo Scientific) along with 0.5 M EDTA and lysed for 20 min on ice. Then, the lysates were sonicated, centrifuged at 10,000 rpm for 10 min at 4°C and the supernatants were collected for further analysis. The protein concentration was determined using a Micro BCA™ Protein Assay Kit (Thermo Scientific) according to the manufacturer's instructions. Equal amounts of the proteins (20 µg) were electrophoresed on SDS-Page gels and transferred onto a nitrocellulose membranes. The membranes were blocked in 5% non-fat milk that was prepared in PBS containing 0.1% Tween-20 (TPBS) for 1 h. After blocking, the membranes were incubated with specific primary antibodies: cdc2, p21^{Waf1/Cip1}, p53, cyclin D1, cytochrome c, PARP, α-tubulin and β-actin overnight at 4°C, and then washed and incubated with horseradish peroxidase (HRP)-conjugated secondary antibodies for 1 h at room temperature. All of the antibodies were purchased from CellSignaling (Danvers, MA, USA) and were diluted 1:1000 in 5% milk in TPBS. Finally, the membranes were washed and incubated with a SuperSignal™ West Pico Chemiluminescent Substrate (Thermo Scientific). The chemiluminescence signals were captured using a ChemiDoc™ XRS+ System (BioRad). The experiments were performed at least three times.

4.2.8. Cell cycle assay

The HCT 116 p53^{+/+}, MCF-7 and U-251 cells were seeded in 3 cm Petri dishes (Nunc) at a density of $0.25 \cdot 10^6$ cells/well and incubated at 37°C for 24 h. Then, the medium was removed and freshly prepared solutions of the tested compounds, **1c**, **1e**, **2a-c**, **3c**, **3e**, **3h**, at a 0.5 µM concentration were added. After a 48-h treatment, the assays were performed using a Muse Cell-Cycle Kit (Millipore) according to the manufacturer's instructions. Briefly, the cells were collected, washed with cold PBS and centrifuged at 300 g. Then, the cells were fixed in ice cold 70% ethanol and stored at -20°C overnight, after which the cells were

centrifuged and resuspended in 200 μL of the Muse™ Cell Cycle Reagent and incubated for 30 min at room temperature in the dark. After staining, the cells were processed for cell cycle analysis using a Muse Cell Analyzer (Millipore). The experiments were performed at least three times.

4.2.9. Annexin V binding assay

The HCT 116 p53^{+/+}, MCF-7 and U-251 cells were seeded in 3 cm Petri dishes (Nunc) at a density of $0.25 \cdot 10^6$ cells/well and incubated at 37°C for 24 h. Then, the medium was removed and freshly prepared solutions of the tested compounds, **1c**, **1e**, **2a-c**, **3c**, **3e**, **3h**, at a 0.5 μM concentration were added. After 48 h, the assays were performed using an Annexin V & Dead Cell Kit (Millipore) according to the manufacturer's instructions. Briefly, detached and adherent cells were collected and centrifuged at 500 g for 5 min, after which the resuspended cells were incubated with 100 μL of the Muse™ Annexin V & Dead Cell Reagent for 20 min at room temperature in the dark. After staining, the events for the live, early and late apoptotic cells were counted using a Muse Cell Analyzer (Millipore). The experiments were performed at least three times.

4.2.10. Intercalation

For the DNA binding studies, Calf-thymus DNA (CT-DNA) was purchased from Sigma Aldrich. The lyophilized CT-DNA was dissolved in 10 mM Tris-HCl, pH 7.9, mixed gently and left overnight at 4°C. The purity of the CT-DNA solution was determined by measuring the ratio of the UV absorbance at 260 and 280 nm. A ratio of more than 1.8 indicated that the DNA was sufficiently free from proteins. Then, the concentration of CT-DNA was determined from the absorbance at 260 nm using an extinction coefficient of $6,600 \text{ M}^{-1}\text{cm}^{-1}$. The tested TSC (**1c**, **1e**, **2b-c**, **3c**, **3e**, **3g-i**, **Dp44mT**) and **DOX** were dissolved in DMSO to a concentration of 8.35 mM, which was then used as the stock solution for preparing the various concentrations (25, 12.5, 6 and 3 μM) in 1 mL in 10 mM of Tris-HCl (pH 7.9). Afterwards, 18 μM CT-DNA was added to the prepared solutions, which were then incubated for 1.5 h at 37°C with occasional vortexing. The absorption spectra were measured using a Hitachi U-2900 spectrophotometer in the range of 200-500 nm. All of 6600 absorption spectra were imported and compared in OriginPro 8.0.

4.2.11. Statistical analysis

The results are expressed as the mean \pm standard deviation (SD) from at least three independent experiments. Statistical analysis was performed using the one-way ANOVA with a Bonferroni post-hoc test. A p-value of 0.05 or less was considered to be statistically significant. GraphPad Prism v.7.0 software (GraphPad Software, USA) was used for the analysis.

Author contributions

AMW created the research hypothesis; AMW and KM designed and performed the biological tests; MR carried out the chemical syntheses supervised by JP; JP and KM edited the text; AMW and RM wrote the manuscript.

Acknowledgements

The financial support of the National Science Centre grants 2014/13/D/NZ7/00322 (A.M.W.) and 2016/23/N/NZ7/00351 (K.M.) was greatly appreciated.

References

- [1] H. Beraldo and D. Gambino, "The wide pharmacological versatility of semicarbazones, thiosemicarbazones and their metal complexes.," *Mini Rev. Med. Chem.*, vol. 4, no. 1, pp. 31–9, Jan. 2004.
- [2] Y. Aye, M. J. C. Long, and J. Stubbe, "Mechanistic studies of semicarbazone triapine targeting human ribonucleotide reductase in vitro and in mammalian cells: Tyrosyl radical quenching not involving reactive oxygen species," *J. Biol. Chem.*, vol. 287, no. 42, pp. 35768–35778, 2012.
- [3] S. Attia, J. Kolesar, M. R. Mahoney, H. C. Pitot, D. Laheru, J. Heun, W. Huang, J. Eickhoff, C. Erlichman, and K. D. Holen, "A phase 2 consortium (P2C) trial of 3-aminopyridine-2-carboxaldehyde thiosemicarbazone (3-AP) for advanced adenocarcinoma of the pancreas.," *Invest. New Drugs*, vol. 26, no. 4, pp. 369–79, Aug. 2008.
- [4] K. Y. Salim, S. M. Vareki, W. R. Danter, S. San-Marina, and J. Koropatnick, "COTI-2, a novel small molecule that is active against multiple human cancer cell lines *in vitro*

- and *in vivo*,” *Oncotarget*, vol. 7, no. 27, Jul. 2016.
- [5] Y. Yu, Y. S. Rahmanto, C. L. Hawkins, and D. R. Richardson, “The Potent and Novel Thiosemicarbazone Chelators Di-2- Crucial Thiol Systems Required for Ribonucleotide Reductase,” 2011.
- [6] V. A. Rao, S. R. Klein, K. K. Agama, E. Toyoda, N. Adachi, Y. Pommier, and E. B. Shacter, “The iron chelator Dp44mT causes DNA damage and selective inhibition of topoisomerase IIalpha in breast cancer cells,” *Cancer Res.*, vol. 69, no. 3, pp. 948–57, 2009.
- [7] K. Malarz, A. Mrozek-Wilczkiewicz, M. Serda, M. Rejmund, J. Polanski, and R. Musiol, “The role of oxidative stress in activity of anticancer thiosemicarbazones,” *Oncotarget*, vol. 9, no. 25, pp. 477–486, Apr. 2018.
- [8] M. Rejmund, A. Mrozek-Wilczkiewicz, K. Malarz, M. Pyrkosz-Bulska, K. Gajcy, M. Sajewicz, R. Musiol, and J. Polanski, “Piperazinyl fragment improves anticancer activity of Triapine,” *PLoS One*, vol. 13, no. 4, p. e0188767, Apr. 2018.
- [9] M. Whitnall, J. Howard, P. Ponka, and D. R. Richardson, “A class of iron chelators with a wide spectrum of potent antitumor activity that overcomes resistance to chemotherapeutics,” *Proc. Natl. Acad. Sci. U. S. A.*, vol. 103, no. 40, pp. 14901–6, Oct. 2006.
- [10] D. B. Lovejoy and D. R. Richardson, “Novel ‘hybrid’ iron chelators derived from aroylhydrazones and thiosemicarbazones demonstrate selective antiproliferative activity against tumor cells,” *Blood*, vol. 100, no. 2, pp. 666–676, Jun. 2002.
- [11] P. Heffeter, V. F. S. S. Pape, É. A. Enyedy, B. K. Keppler, G. Szakacs, C. R. Kowol, E. A. Enyedy, B. K. Keppler, G. Szakas, and C. R. Kowol, “Anticancer thiosemicarbazones: chemical properties, interaction with iron metabolism, and resistance development,” *Antioxid. Redox Signal.*, vol. 30, no. 8, p. ars.2017.7487, Mar. 2018.
- [12] R. T. Dean and P. Nicholson, “The action of nine chelators on iron-dependent radical damage,” *Free Radic. Res.*, vol. 20, no. 2, pp. 83–101, Feb. 1994.
- [13] G. Link, A. M. Konijn, and C. Hershko, “Cardioprotective effect of alpha-tocopherol, ascorbate, deferoxamine, and deferiprone: mitochondrial function in cultured, iron-loaded heart cells,” *J. Lab. Clin. Med.*, vol. 133, no. 2, pp. 179–88, Feb. 1999.
- [14] D. B. Lovejoy, P. J. Jansson, U. T. Brunk, J. Wong, P. Ponka, and D. R. Richardson, “Antitumor activity of metal-chelating compound Dp44mT is mediated by formation of a redox-active copper complex that accumulates in lysosomes,” *Cancer Res.*, vol. 71,

- no. 17, pp. 5871–5880, 2011.
- [15] K. Ishiguro, Z. P. Lin, P. G. Penketh, K. Shyam, R. Zhu, R. P. Baumann, Y.-L. Zhu, A. C. Sartorelli, T. J. Rutherford, and E. S. Ratner, “Distinct mechanisms of cell-kill by triapine and its terminally dimethylated derivative Dp44mT due to a loss or gain of activity of their copper(II) complexes,” *Biochem. Pharmacol.*, vol. 91, no. 3, pp. 312–322, Oct. 2014.
- [16] J. C. Yalowich, X. Wu, R. Zhang, R. Kanagasabai, M. Hornbaker, and B. B. Hasinoff, “The anticancer thiosemicarbazones Dp44mT and triapine lack inhibitory effects as catalytic inhibitors or poisons of DNA topoisomerase II α ,” *Biochem. Pharmacol.*, vol. 84, no. 1, pp. 52–58, Jul. 2012.
- [17] Y. Yu, E. Gutierrez, Z. Kovacevic, F. Saletta, P. Obeidy, Y. Suryo Rahmanto, and D. R. Richardson, “Iron Chelators for the Treatment of Cancer,” *Curr. Med. Chem.*, vol. 19, no. 17, pp. 2689–2702, 2012.
- [18] D. R. Richardson, P. C. Sharpe, D. B. Lovejoy, D. Senaratne, D. S. Kalinowski, M. Islam, and P. V Bernhardt, “Dipyridyl thiosemicarbazone chelators with potent and selective antitumor activity form iron complexes with redox activity.,” *J. Med. Chem.*, vol. 49, no. 22, pp. 6510–21, Nov. 2006.
- [19] A. Mrozek-Wilczkiewicz, M. Serda, R. Musiol, G. Malecki, A. Szurko, A. Muchowicz, J. Golab, A. Ratuszna, and J. Polanski, “Iron chelators in photodynamic therapy revisited: synergistic effect by novel highly active thiosemicarbazones.,” *ACS Med. Chem. Lett.*, vol. 5, no. 4, pp. 336–9, Apr. 2014.
- [20] M. Serda, D. S. Kalinowski, N. Rasko, E. Potůčková, A. Mrozek-Wilczkiewicz, R. Musiol, J. G. Małecki, M. Sajewicz, A. Ratuszna, A. Muchowicz, J. Gołąb, T. Simůnek, D. R. Richardson, and J. Polanski, “Exploring the Anti-Cancer Activity of Novel Thiosemicarbazones Generated through the Combination of Retro-Fragments: Dissection of Critical Structure-Activity Relationships.,” *PLoS One*, vol. 9, no. 10, p. e110291, Jan. 2014.
- [21] M. Serda, D. S. Kalinowski, A. Mrozek-Wilczkiewicz, R. Musiol, A. Szurko, A. Ratuszna, N. Pantarat, Z. Kovacevic, A. M. Merlot, D. R. Richardson, and J. Polanski, “Synthesis and characterization of quinoline-based thiosemicarbazones and correlation of cellular iron-binding efficacy to anti-tumor efficacy,” *Bioorg. Med. Chem. Lett.*, vol. 22, no. 17, pp. 5527–5531, Sep. 2012.
- [22] M. Serda, A. Mrozek-Wilczkiewicz, J. Jampilek, M. Pesko, K. Kralova, M. Vejsova, R. Musiol, A. Ratuszna, and J. Polanski, “Investigation of the Biological Properties of

- (Hetero)Aromatic Thiosemicarbazones,” *Molecules*, vol. 17, no. 11, pp. 13483–13502, Nov. 2012.
- [23] D. S. Kalinowski, Y. Yu, P. C. Sharpe, M. Islam, Y.-T. Liao, D. B. Lovejoy, N. Kumar, P. V Bernhardt, and D. R. Richardson, “Design, synthesis, and characterization of novel iron chelators: structure-activity relationships of the 2-benzoylpyridine thiosemicarbazone series and their 3-nitrobenzoyl analogues as potent antitumor agents.,” *J. Med. Chem.*, vol. 50, no. 15, pp. 3716–29, Jul. 2007.
- [24] D. S. Kalinowski, P. C. Sharpe, P. V Bernhardt, and D. R. Richardson, “Structure-activity relationships of novel iron chelators for the treatment of iron overload disease: the methyl pyrazinylketone isonicotinoyl hydrazone series.,” *J. Med. Chem.*, vol. 51, no. 2, pp. 331–44, Jan. 2008.
- [25] C. Stefani, G. Punnia-Moorthy, D. B. Lovejoy, P. J. Jansson, D. S. Kalinowski, P. C. Sharpe, P. V Bernhardt, and D. R. Richardson, “Halogenated 2’-benzoylpyridine thiosemicarbazone (XBpT) chelators with potent and selective anti-neoplastic activity: relationship to intracellular redox activity.,” *J. Med. Chem.*, vol. 54, no. 19, pp. 6936–48, Oct. 2011.
- [26] Z. Kovacevic, S. Chikhani, D. B. Lovejoy, and D. R. Richardson, “Novel Thiosemicarbazone Iron Chelators Induce Up-Regulation and Phosphorylation of the Metastasis Suppressor N-myc Down-Stream Regulated Gene 1: A New Strategy for the Treatment of Pancreatic Cancer,” *Mol. Pharmacol.*, vol. 80, no. 4, pp. 598–609, Oct. 2011.
- [27] Y. Yu, D. S. Kalinowski, Z. Kovacevic, A. R. Siafakas, P. J. Jansson, C. Stefani, D. B. Lovejoy, P. C. Sharpe, P. V Bernhardt, and D. R. Richardson, “Thiosemicarbazones from the old to new: iron chelators that are more than just ribonucleotide reductase inhibitors.,” *J. Med. Chem.*, vol. 52, no. 17, pp. 5271–94, Sep. 2009.
- [28] K. Y. Salim, S. Maleki Vareki, W. R. Danter, and J. Koropatnick, “COTI-2, a novel small molecule that is active against multiple human cancer cell lines in vitro and in vivo.,” *Oncotarget*, vol. 7, no. 27, pp. 41363–41379, Jul. 2016.
- [29] R. T. Ho, K. Y. Salim, A. Lindemann, A. A. Patel, H. Takahashi, L. Wang, M. Zhao, S. J. Frank, J. Myers, A. A. Osman, C. Lynam, and A. D. Silva, “COTI-2, a potent orally available small molecule targeting mutant p53, with promising efficacy as monotherapy and combination treatment in preclinical tumor models.,” *J. Clin. Oncol.*, vol. 36, no. 15_suppl, pp. 6040–6040, May 2018.
- [30] Y. Zhang, C. Dube, M. Gibert, N. Cruickshanks, B. Wang, M. Coughlan, Y. Yang, I.

- Setiady, C. Deveau, K. Saoud, C. Grello, M. Oxford, F. Yuan, and R. Abounader, "The p53 Pathway in Glioblastoma," *Cancers (Basel)*, vol. 10, no. 9, p. 297, Sep. 2018.
- [31] M. Brázdová, T. Quante, L. Tögel, K. Walter, C. Loscher, V. Tichý, L. Činčárová, W. Deppert, and G. V. Tolstonog, "Modulation of gene expression in U251 glioblastoma cells by binding of mutant p53 R273H to intronic and intergenic sequences," *Nucleic Acids Res.*, vol. 37, no. 5, pp. 1486–1500, Apr. 2009.
- [32] A. Mrozek-Wilczkiewicz, K. Malarz, M. Rams-Baron, M. Serda, D. Bauer, F.-P. Montforts, A. Ratuszna, T. Burley, J. Polanski, and R. Musiol, "Iron Chelators and Exogenic Photosensitizers. Synergy through Oxidative Stress Gene Expression," *J. Cancer*, vol. 8, no. 11, pp. 1979–1987, 2017.
- [33] P. J. Jansson, P. C. Sharpe, P. V Bernhardt, and D. R. Richardson, "Novel thiosemicarbazones of the ApT and DpT series and their copper complexes: identification of pronounced redox activity and characterization of their antitumor activity.," *J. Med. Chem.*, vol. 53, no. 15, pp. 5759–69, Aug. 2010.
- [34] D. B. Lovejoy, D. M. Sharp, N. Seebacher, P. Obeidy, T. Prichard, C. Stefani, M. T. Basha, P. C. Sharpe, P. J. Jansson, D. S. Kalinowski, P. V Bernhardt, and D. R. Richardson, "Novel second-generation di-2-pyridylketone thiosemicarbazones show synergism with standard chemotherapeutics and demonstrate potent activity against lung cancer xenografts after oral and intravenous administration in vivo.," *J. Med. Chem.*, vol. 55, no. 16, pp. 7230–44, Aug. 2012.
- [35] A. E. Stacy, D. Palanimuthu, P. V. Bernhardt, D. S. Kalinowski, P. J. Jansson, and D. R. Richardson, "Structure-Activity Relationships of Di-2-pyridylketone, 2-Benzoylpyridine, and 2-Acetylpyridine Thiosemicarbazones for Overcoming Pgp-Mediated Drug Resistance," *J. Med. Chem.*, vol. 59, no. 18, pp. 8601–8620, 2016.
- [36] E. M. Gutierrez, N. A. Seebacher, L. Arzuman, Z. Kovacevic, D. J. R. Lane, V. Richardson, A. M. Merlot, H. Lok, D. S. Kalinowski, S. Sahni, P. J. Jansson, and D. R. Richardson, "Lysosomal membrane stability plays a major role in the cytotoxic activity of the anti-proliferative agent, di-2-pyridylketone 4,4-dimethyl-3-thiosemicarbazone (Dp44mT)," *Biochim. Biophys. Acta - Mol. Cell Res.*, vol. 1863, no. 7, pp. 1665–1681, 2016.
- [37] E. Gutierrez, D. R. Richardson, and P. J. Jansson, "The anticancer agent di-2-pyridylketone 4,4-dimethyl-3-thiosemicarbazone (Dp44mT) overcomes prosurvival autophagy by two mechanisms: persistent induction of autophagosome synthesis and impairment of lysosomal integrity.," *J. Biol. Chem.*, vol. 289, no. 48, pp. 33568–89,

- Nov. 2014.
- [38] S. Hager, K. Korbula, B. Bielec, M. Grusch, C. Pirker, M. Schosserer, L. Liendl, M. Lang, J. Grillari, K. Nowikovsky, V. F. S. Pape, T. Mohr, G. Szakács, B. K. Keppler, W. Berger, C. R. Kowol, and P. Heffeter, “The thiosemicarbazone Me2NNMe2 induces paraptosis by disrupting the ER thiol redox homeostasis based on protein disulfide isomerase inhibition,” *Cell Death Dis.*, vol. 9, no. 11, p. 1052, 2018.
- [39] R. S. Moussa, K. C. Park, Z. Kovacevic, and D. R. Richardson, “Ironing out the role of the cyclin-dependent kinase inhibitor, p21 in cancer: Novel iron chelating agents to target p21 expression and activity,” *Free Radic. Biol. Med.*, no. December 2017, pp. 1–19, 2018.
- [40] K. Fukuchi, S. Tomoyasu, H. Watanabe, S. Kaetsu, N. Tsuruoka, and K. Gomi, “Iron deprivation results in an increase in p53 expression,” *Biol. Chem. Hoppe. Seyler.*, vol. 376, no. 10, pp. 627–30, Oct. 1995.
- [41] N. C. Synnott, D. J. O’Connell, J. Crown, and M. J. Duffy, “Targeting mutant p53 with COTI-2: A new approach for the treatment of patients with triple-negative breast cancer?,” *J. Clin. Oncol.*, vol. 36, no. 15_suppl, pp. e13121–e13121, May 2018.
- [42] A. Mrozek-Wilczkiewicz, E. Spaczynska, K. Malarz, W. Cieslik, M. Rams-Baron, V. Kryštof, and R. Musiol, “Design, Synthesis and In Vitro Activity of Anticancer Styrylquinolines. The p53 Independent Mechanism of Action,” *PLoS One*, vol. 10, no. 11, p. e0142678, Nov. 2015.
- [43] W. G. An, M. Kanekal, M. C. Simon, E. Maltepe, M. V Blagosklonny, and L. M. Neckers, “Stabilization of wild-type p53 by hypoxia-inducible factor 1alpha,” *Nature*, vol. 392, no. 6674, pp. 405–408, 1998.
- [44] R. Margueron, A. Licznar, G. Lazennec, F. Vignon, and V. Cavaillès, “Oestrogen receptor α increases p21WAF1/CIP1 gene expression and the antiproliferative activity of histone deacetylase inhibitors in human breast cancer cells,” *J. Endocrinol.*, vol. 179, no. 1, pp. 41–53, 2003.
- [45] R. S. Moussa, Z. Kovacevic, D. H. Bae, D. J. R. Lane, and D. R. Richardson, “Transcriptional regulation of the cyclin-dependent kinase inhibitor, p21CIP1/WAF1, by the chelator, Dp44mT,” *Biochim. Biophys. Acta - Gen. Subj.*, vol. 1862, no. 3, pp. 761–774, 2017.
- [46] N. Sanvisens, M. C. Bañó, M. Huang, and S. Puig, “Regulation of ribonucleotide reductase in response to iron deficiency,” *Mol. Cell*, vol. 44, no. 5, pp. 759–769, 2011.
- [47] D. Candas, M. Fan, D. Nantajit, A. T. Vaughan, J. S. Murley, G. E. Woloschak, D. J.

- Grđina, and J. J. Li, "CyclinB1/Cdk1 phosphorylates mitochondrial antioxidant MnSOD in cell adaptive response to radiation stress," *J. Mol. Cell Biol.*, vol. 5, no. 3, pp. 166–175, 2013.
- [48] A. Gęgotek, M. Cyuńczyk, W. Łuczaj, A. Bielawska, K. Bielawski, and E. Skrzydlewska, "The redox status of human breast cancer cell lines (MCF-7 and MDA-MB231) treated with novel dinuclear berenil-platinum(II) complexes.," *Pharmazie*, vol. 69, no. 12, pp. 923–8, Dec. 2014.
- [49] G. Haklar, E. Sayin-Özveri, M. Yüksel, A. Ö. Aktan, and A. S. Yalçın, "Different kinds of reactive oxygen and nitrogen species were detected in colon and breast tumors," *Cancer Lett.*, vol. 165, no. 2, pp. 219–224, Apr. 2001.
- [50] S. S. Thorgeirsson, "Endogenous DNA damage and breast cancer," *Cancer*, vol. 71, no. 10, pp. 2897–2899, 1993.
- [51] C. Gorrini, I. S. Harris, and T. W. Mak, "Modulation of oxidative stress as an anticancer strategy," *Nat. Rev. Drug Discov.*, vol. 12, no. 12, pp. 931–947, 2013.
- [52] S. Tardito, I. Bassanetti, C. Bignardi, L. Elviri, M. Tegoni, C. Mucchino, O. Bussolati, R. Franchi-Gazzola, and L. Marchiò, "Copper binding agents acting as copper ionophores lead to caspase inhibition and paraptotic cell death in human cancer cells," *J. Am. Chem. Soc.*, vol. 133, no. 16, pp. 6235–6242, 2011.
- [53] U. Jungwirth, C. R. Kowol, B. K. Keppler, C. G. Hartinger, W. Berger, and P. Heffeter, "Anticancer Activity of Metal Complexes: Involvement of Redox Processes," *Antioxid. Redox Signal.*, vol. 15, no. 4, pp. 1085–1127, Aug. 2011.
- [54] P. V Bernhardt, M. Martínez, C. Rodríguez, and M. Vazquez, "Biologically active thiosemicarbazone Fe chelators and their reactions with ferrioxamine B and ferric EDTA; a kinetic study.," *Dalton Trans.*, vol. 41, no. 7, pp. 2122–30, Feb. 2012.
- [55] T. R. Dunkern, I. Wedemeyer, M. Baumgärtner, G. Fritz, and B. Kaina, "Resistance of p53 knockout cells to doxorubicin is related to reduced formation of DNA strand breaks rather than impaired apoptotic signaling.," *DNA Repair (Amst.)*, vol. 2, no. 1, pp. 49–60, Jan. 2003.

- Thiosemicarbazone drug candidates impact on the reactive oxygen species generation
- Metal chelators intercalate to DNA and inhibit cell cycle progression
- Thiosemicarbazone derivatives alternate the expression of crucial proteins

ACCEPTED MANUSCRIPT